FEBS Letters 585 (2011) 3310–3315

FEBS Letters

journal homepage: www.FEBSLetters.org

siRNA-mediated knockdown of aryl hydrocarbon receptor nuclear translocator 2 affects hypoxia-inducible factor-1 regulatory signaling and metabolism in human breast cancer cells

Xian-Yang Qin [a,b,1], Feifei Wei [c,1], Jun Yoshinaga [b], Junzo Yonemoto [a], Masaru Tanokura [c], Hideko Sone [a,*]

[a] Health Risk Research Section, Research Center for Environmental Risk, National Institute for Environmental Studies, 16-2 Onogawa, Tsukuba, Ibaraki 305-8506, Japan
[b] Department of Environmental Studies, Graduate School of Frontier Science, The University of Tokyo, 5-1-5 Kashiwanoha, Kashiwa, Chiba 270-8563, Japan
[c] Department of Applied Biological Chemistry, Graduate School of Agricultural and Life Sciences, The University of Tokyo, 1-1-1 Yayoi, Bunkyo-ku, Tokyo 113-8657, Japan

ARTICLE INFO

Article history:
Received 18 August 2011
Revised 9 September 2011
Accepted 13 September 2011
Available online 19 September 2011

Edited by Judit Ovádi

Keywords:
Aryl-hydrocarbon receptor nuclear translocator 2
Breast cancer
Hypoxia-inducible factor-1
Metabolomics
Nuclear magnetic resonance

ABSTRACT

Recent human studies found that the mRNA expression level of aryl-hydrocarbon receptor nuclear translocator 2 (ARNT2) was positively associated with the prognosis of breast cancer. In this study, we used small interfering RNA techniques to knockdown ARNT2 expression in MCF7 human breast cancer cells, and found that an almost 40% downregulation of ARNT2 mRNA expression increased the expression of sensitive to apoptosis gene (3.36-fold), and decreased the expression of von Hippel-Lindau (0.27-fold) and matrix metalloproteinase-1 (0.35-fold). The metabolite analysis revealed the contents of glucose, glycine, betaine, phosphocholine, pyruvate and lactate involved in the hypoxia-inducible factor (HIF)-1-dependent glycolytic pathway were significantly lower in cells treated with siARNT2. Our results suggested that ARNT2 might play an important role in the modulation of HIF-1-regulated signaling and metabolism.

1. Introduction

Aryl-hydrocarbon receptor nuclear translocator 2 (ARNT2) is a member of the basic helix-loop-helix Per-ARNT-SIM family of transcription factors [1] and acts as a common obligate partner for several other members of the family, including aryl hydrocarbon receptor (AHR) and hypoxia-inducible factor (HIF)-1α [2,3]. Although many of the functions of ARNT2 remain unknown, it is believed that ARNT2 plays important roles in tumor angiogenesis by forming functional HIF complexes [4]. A recent study showed that ARNT2 mRNA expression levels are positively correlated with the prognosis of breast cancer, and that the presence of ARNT2 was significantly associated with smaller tumor sizes ($P = 0.006$), relapse-free survival ($P = 0.027$), and overall survival ($P = 0.002$) 5 years after breast cancer diagnosis [5]. These perspective findings indicate a possible role of ARNT2 in cancer development, treatment and outcome; however, much of this has yet to be elucidated.

Metabolites are regarded as the end products of cellular regulatory processes, and their levels can be considered as the ultimate response of biological systems to genetic or environmental changes [6]. The metabolism of a solid tumor is significantly different from that of the surrounding normal tissue, with cancer cells shifting glucose metabolism from oxidative to glycolytic pathways [7]. This process is known as the Warburg effect, at the heart of which is the HIF-dependent (and in particular, HIF-1-dependent) transcriptional regulation of virtually all of the genes in the glycolytic pathway, including glucose transporters, glycolytic enzymes, and various proteins involved in lactate production and pyruvate metabolism [8]. Nuclear magnetic resonance (NMR)-based metabolic profiling and metabolomics, combined with multivariate statistical analysis, have been widely applied in various areas of research, including drug toxicology, biomarker discovery, functional genomics, and molecular pathology [9–13]. Compared to other analytical techniques, such as gas chromatography–mass

Abbreviations: ARNT2, aryl-hydrocarbon receptor nuclear translocator 2; BaP, benzo[*a*]pyrenes; Glut-1, glucose transporter 1; HIF, hypoxia-inducible factor; KEGG, Kyoto Encyclopedia of Genes and Genomes; MMP1, matrix metalloproteinase-1; NMR, nuclear magnetic resonance; OPLS-DA, orthogonal projection to latent structure discriminant analysis; PCA, principal component analysis; SAG, sensitive to apoptosis gene; siRNA, small interfering RNA; VHL, von Hippel-Lindau

* Corresponding author. Fax: +81 29 850 2546.
E-mail addresses: y_qin@envhlth.k.u-tokyo.ac.jp (X.-Y. Qin), aa097025@mail.ecc.u-tokyo.ac.jp (F. Wei), junyosh@k.u-tokyo.ac.jp (J. Yoshinaga), yonemoto@nies.go.jp (J. Yonemoto), amtanok@mail.ecc.u-tokyo.ac.jp (M. Tanokura), hsone@nies.go.jp (H. Sone).

[1] These two authors contributed equally to this work.

0014-5793/$36.00
doi:10.1016/j.febslet.2011.09.017

spectrometry or liquid chromatography–mass spectrometry, NMR has the advantage of a fully quantitative analysis (with minimal sample preparation) to achieve a quick, direct and comprehensive observation [14].

In this study, NMR-based metabolomics was employed to investigate whether dysregulated ARNT2 mRNA expression could affect HIF-1-regulated metabolism in MCF7 human breast cancer cells. To assess the potential function of ARNT2 in breast cancer, we utilized small interfering RNA (siRNA) to knockdown ARNT2 mRNA expression levels in MCF7 cells, and then investigated its effect on the HIF-1 regulated signaling and metabolism.

2. Materials and methods

2.1. Cell culture

MCF7 cells were obtained from the Cell Engineering Division of RIKEN BioResource Center (Tsukuba, Ibaraki, Japan). Cells were maintained in RPMI 1640 medium (Wako, Osaka, Japan) containing 10% fetal bovine serum (FBS) (Mediatech, Herndon, VA) and grown at 37 °C in a 5% CO_2 humidified incubator. For growth under steroid-free conditions, the cells were seeded in phenol red-free DMEM (MP Biomedicals, Solon, OH) containing 10% charcoal/dextran-treated FBS (Hyclone, Logan, UT). All culture media contained 100 U/ml penicillin/streptomycin and 2 mmol/l L-glutamine (Mediatech).

2.2. RNA interference

siRNA targeting human ARNT2 (5′-CCGAUGGAAUCAUCACAUUUU-3′) and a scrambled sequence were designed and purchased from Genolution Pharmaceuticals Inc. (Seoul, South Korea). MCF7 cells were plated in 96-well plates (1×10^4 cells/well) for cell viability analysis, 24-well plates (5×10^4 cells/well) for RNA isolation, and 100 mm dishes (1×10^6 cells/dish) for metabolite analysis in phenol red-free media 1 day prior to transfection. Cells were then transfected with 10 nM or 100 nM siARNT2 and the scrambled siRNA as a negative control using G-Fectin, as per the manufacturer's instructions (Genolution Pharmaceuticals). The transfected cells were then incubated at 37 °C for 72 h and cultured in phenol red-free media without siARNT2 for another 48 h before analysis.

2.3. Quantitative real-time reverse transcription-polymerase chain reaction (RT-PCR)

Total RNA was isolated from cell cultures using an RNeasy Kit (Qiagen, Valencia, CA), and their amounts, purity and integrity were evaluated using a UV spectrophotometer and an Agilent Bioanalyzer 2100 (Agilent Technologies, Palo Alto, CA). cDNA was then synthesized using a High Capacity RNA-to-cDNA Kit (Applied Biosystems, Foster City, CA) and amplified in triplicate using TaqMan® Gene Expression Master Mix (Applied Biosystems) as previously described [15]. TaqMan Gene Expression Assays (Applied Biosystems) used in this study were Hs00208298_m1 for ARNT2, Hs00231048_m1 for ARNT, and Hs99999903_m1 for beta-actin. The gene expression was normalized to beta-actin expression and set to 1.0 for control cells treated with scramble siRNA.

2.4. Cell viability assay

Cells were washed twice with cold phosphate-buffered saline (PBS, Gibco, Grand Island, NY) and then fixed in 4% neutralized paraformaldehyde solution for 30 min. Nuclear counter-staining was detected with Hoechst 33258 (Wako Pure Chemical Industries, Osaka, Japan) and high-content cellular fluorescence images were acquired using an automatic fluorescence microscope (IN Cell Analyzer 1000; GE Healthcare, Buckinghamshire, UK).

2.5. Human HIF-regulated cDNA plate array

A human HIF-regulated cDNA plate array was used to determine the effect of downregulated ARNT2 mRNA expression on HIF-1 signaling (AP-0111, Signosis Inc., Sunnyvale, CA), according to the manufacturer's instructions. Briefly, total RNA (2 μg) was first reverse transcribed into cDNA in the presence of biotin-dUTP. Target genes were then specifically captured to individual wells on the plate through a pre-coated gene-specific oligonucleotide. The captured cDNAs were then detected with streptavidin-horseradish peroxidase (HRP) by the addition of a HRP chemiluminescent substrate. The concentration of cDNA was directly proportional to the chemiluminescent intensity of the test sample. The luciferase activity was measured using an AB-2100 luminometer (Atto, Tokyo, Japan). Luciferase induction was normalized to beta-actin and set to 1.0 for control cells treated with scramble siRNA.

2.6. NMR sample preparation

For metabolite analysis, MCF7 cells were harvested, as previously reported [16]. Briefly, cells (approximately 1×10^7 cells) were pelleted and washed twice with cold PBS to remove any residual medium. Excess PBS was removed via two rounds of centrifugation at maximum speed. Cell pellets were then stored at −80 °C for subsequent extraction. Aqueous soluble metabolites were then extracted using a chloroform/methanol/water extraction method, as previously described [13].

2.7. NMR analysis

The one-dimensional (1D) ^{1}H NMR spectra were measured at 500 MHz on a Varian Unity INOVA-500 spectrometer. The H_2O signal was suppressed by the pre-saturation method. The acquisition parameters were as follows: number of data points, 64 k; spectral width, 8000 Hz; acquisition time, 4.000 s; delay time, 2.0 s; and number of scans, 256. Detailed methods have been described previously [17].

2.8. Processing of spectra and data reduction

All NMR spectra were processed with the program MestReNova (Version 5.3.0, MestReC, Santiago de Compostela, Spain), reduced into 0.04 ppm spectral buckets, aligned using the Correlation Optimized Warping method, and then normalized.

2.9. Identification of metabolites

Metabolites were identified in the NMR spectra by comparing their ^{1}H chemical shifts and coupling patterns with corresponding values of metabolites from publicly accessible data banks [12], including the BioMagRes data bank (http://www.bmrb.wisc.edu), the Metabolomics Database of Linkoping (http://www.mdl.imv.liu.se), and the Human Metabolome Data Bank (http://www.hmdb.ca).

2.10. Statistical and multivariate analysis

All experiments in this study were performed in triplicate to test the reproducibility of the results. Quantitative data were expressed as the mean ± S.D. Statistical analysis was performed by two-tailed Student's *t*-test. Relationships were considered statistically significant with $P < 0.05$. Unsupervised principal component analysis (PCA) was used to obtain a general overview of the variance of the metabolites, and supervised orthogonal projection

to latent structure discriminant analysis (OPLS-DA) was performed to obtain information about differences in the metabolite composition of samples in SIMCA-P+ (Version 12.0, Umetrics, Umeå, Sweden). The map of the metabolic pathways was obtained from the Kyoto Encyclopedia of Genes and Genomes (KEGG; http://www.genome.jp/kegg/), a publicly available, web-based tool.

3. Results

3.1. Knockdown of ARNT2 mRNA expression in MCF7 cells

This study focused on the potential function of ARNT2 in human breast cancer cells. First, we sought to downregulate the mRNA expression of ARNT2 in MCF7 cells using siRNA techniques, the effects of which were confirmed by gene expression analysis and a cell viability assay. As shown in Fig. 1A, siARNT2 treatment caused a dose-dependent downregulation of ARNT2 mRNA expression. When treated with 10 and 100 nM siARNT2 for 72 h, we observed nearly 40% and 60% reductions, respectively, in ARNT2 mRNA expression in MCF7 cells. No significant effect was observed in ARNT mRNA expression with siARNT2 treatment (Fig. 1A). Furthermore, according to the cell viability assay, a significant inhibition in cell growth (approximately 80%) was observed in MCF7 cells treated with 100 nM, but not 10 nM, siARNT2 for 72 h (Fig. 1B). Hoechst staining indicated that a high dose of siARNT2 treatment at 100 nM induced apoptosis in MCF7 cells (data not shown).

To avoid cytotoxicity, 10 nM siARNT2 was used in subsequent experiments to investigate the effects of ARNT2 mRNA downregulation on HIF-1-regulated signaling and metabolism in MCF7 cells.

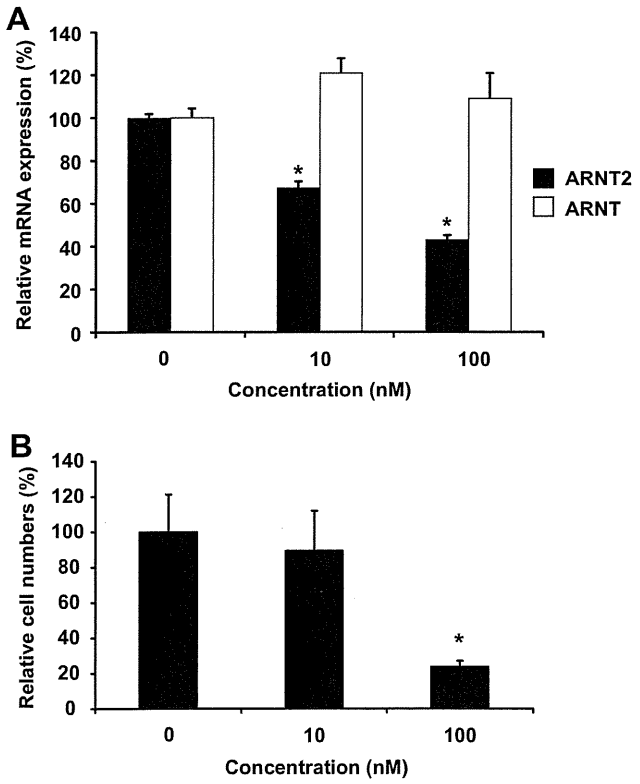

Fig. 1. siRNA-mediated downregulation of ARNT2 mRNA expression in MCF7 cells. Cells were treated with 10 and 100 nM siARNT2 for 72 h and then cultured for another 48 h in steroid-free media without siARNT2 treatment. Dose-dependent decreases in ARNT2 mRNA expression (A) and cell viability (B) following the siARNT2 treatment were confirmed. No significant effect was observed in ARNT mRNA expression with siARNT2 treatment (A). *$P < 0.05$ vs. the control cells treated with scramble siRNA.

3.2. Effects of ARNT2 mRNA downregulation in the expression of HIF signaling genes

A human HIF-regulated cDNA plate assay was used to measure the expression of HIF-1-regulated genes. The plate comprised a total of 21 genes involved in HIF-1 signaling. As shown in Fig. 2, downregulation of ARNT2 mRNA expression by 10 nM siARNT2 treatment for 72 h led to a 3.36-fold induction of sensitive to apoptosis gene (SAG) expression, and a 2-fold induction of Leptin expression. Furthermore, we observed a 0.27-fold and 0.35-fold reduction in von Hippel-Lindau (VHL) and matrix metalloproteinase-1 (MMP1) gene expression, respectively, as well as 0.5-fold reductions in glucose transporter 1 (Glut-1), Glut-3 and HIF-1α genes. These results indicated that ARNT2 may be involved in the modulation of HIF-1 signaling in MCF7 cells.

3.3. Metabolite profiling of MCF7 cells by ^{1}H NMR

A representative 1D ^{1}H NMR spectra of MCF7 cells without any treatment is shown (Fig. 3). Most of the information is located in the upfield region between 0.7 and 4.7 ppm (Fig. 3A), which corresponds to low molecular weight endogenous metabolites. The major metabolite classes observed included amino acids (e.g., alanine, valine, and tyrosine), organic osmolytes (e.g., betaine and glycine), organic acids (e.g., acetic acid), carbohydrates (e.g., glucose), nucleotides (e.g., ATP), and glycolytic products (e.g., lactate and pyruvate).

3.4. Effects of downregulation of ARNT2 mRNA expression in the metabolism of MCF7 cells

To determine which metabolites significantly correlated with the downregulation of ARNT2 mRNA expression, PCA and OPLS-DA modelings were applied to the ^{1}H NMR spectra of six independent data sets from control cells and cells with siARNT2 treatment ($n = 3$, respectively). PCA is a standard technique of pattern recognition and multivariate data analysis. The scores plot (PC 1 vs. 2) discriminated between the intracellular metabolites of control cells and cells treated with siARNT2 (Fig. 4A). It should be noted that these differences were identified using an unsupervised analysis, without any prior information about the samples. Since all

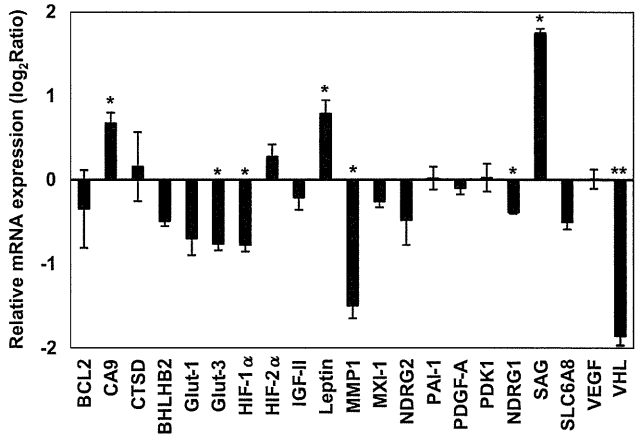

Fig. 2. Effects of downregulation of ARNT2 mRNA expression in the expression of HIF signaling genes in MCF7 cells. Cells were treated with 10 nM siARNT2 for 72 h and then cultured for another 48 h in steroid-free media without siARNT2 treatment. The expression of HIF signaling genes was then measured using a human HIF-regulated cDNA plate assay (Signosis). Relative mRNA expression normalized to beta-actin was shown as $\log_2$ ratio, with the fold-change referring to the control cells. *$P < 0.05$, **$P < 0.01$ vs. the control cells treated with scramble siRNA.

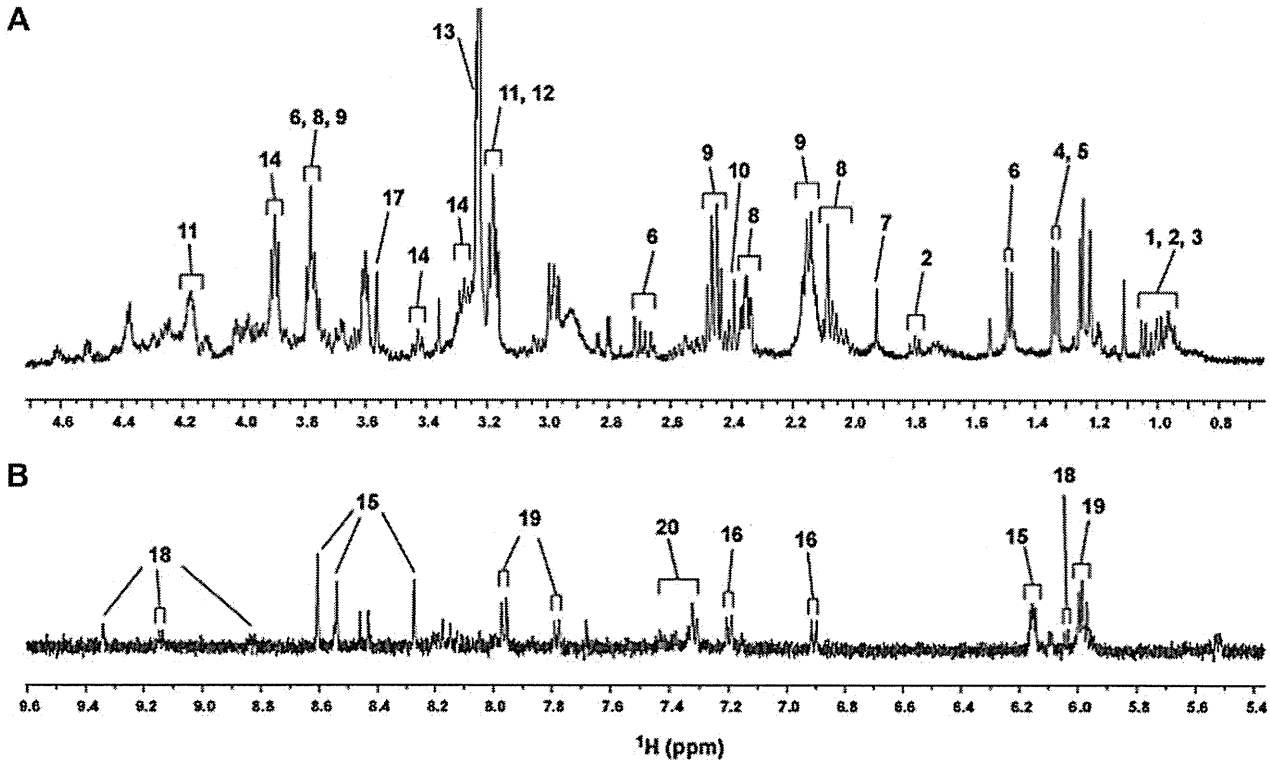

Fig. 3. Assignment of 1D NMR spectra of MCF7 cells. (A) Expansion of the ^{1}H NMR spectrum from 0.7 to 4.7 ppm. (B) Expansion of the ^{1}H NMR spectrum from 5.4 to 9.6 ppm. Metabolites: 1, isoleucine; 2, leucine; 3, valine; 4, lactic acid (lactate); 5, threonine; 6, alanine; 7, acetic acid (acetate); 8, glutamate; 9, glutamine; 10, pyruvic acid (pyruvate); 11, phosphocholine; 12, glycerophosphocholine; 13, betaine; 14, glucose; 15, ATP/ADP/AMP; 16, tyrosine; 17, glycine; 18, NAD+/NADP+; 19, 4-nitrophenol; 20, phenylalanine.

cells were cultured under identical conditions, the observed discrimination demonstrates that the downregulation of ARNT2 mRNA expression is strongly represented by the individual metabolic profiles.

In contrast to PCA, OPLS-DA is a supervised method that explains maximum separation between pre-defined classes in the data. In this case, the scores plot separated control cells and cells treated with siARNT2 along the discriminating t[1] (data not shown). Potential biomarkers for the separation were subsequently identified using S-plot, which were represented with covariance (p) against correlation ($p$corr). The S-plot of the OPLS-DA showed the most relevant variables in the differentiation of two samples, and the identified biomarkers are highlighted in Fig. 4B. The levels of betaine, glucose, glycine, phosphocholine, pyruvate, lactate and ATP/ADP/AMP were significantly decreased in cells with siARNT2 treatment, indicating that the downregulation of ARNT2 mRNA expression may impair HIF-1-regulated glycine synthesis and glucose metabolism in MCF7 cells.

4. Discussion

ARNT2 function is hypothesized to be related to organ development, since Arnt2 knockout mice and zebrafish suffer severe developmental defects and die shortly after birth [18,19]. Compared to its homolog ARNT, ARNT2 is reported to have a more restricted pattern of expression, commonly found in the central nervous system and other developing organs, such as the kidney [4]. However, recent studies have found a increased frequency of ARNT2 transcripts in tumor specimens from primary breast cancer patients, as compared with normal breast tissue samples. Moreover, the mRNA expression levels of ARNT2 correlate significantly with favorable disease outcomes for breast cancer patients, suggesting ARNT2 might be associated with cancer development, treatment and outcome [5]. In this study, we sought to investigate the potential function of ARNT2 in HIF-1-regulated signaling and metabolism in breast cancer, using siRNA to knockdown ARNT2 mRNA expression in MCF7 cells.

HIF-1 regulates numerous pathways that are potentially important for tumor growth, including angiogenesis and glycolysis [20]. Whilst much attention has focused on its role in the cellular response to hypoxia, HIF-1 is also constitutively expressed in many tumors [21]. HIF-1 is a heterodimeric transcription factor composed of HIF-1α, which dimerizes with a constitutively expressed β-subunit, such as ARNT and ARNT2, and subsequently binds to hypoxia response elements in the promoters of target genes [4,8]. HIF-1α expression in cells is known to be regulated by a variety of stimuli, including fluctuations in cellular oxygen concentration, growth factors, oncogenic activation, or loss of tumor suppressor function [22]. In this study, knockdown of ARNT2 mRNA expression significantly decreased HIF-1α expression (0.58-fold, $P = 0.049$), while no significant effect was found with HIF-2α expression (1.25-fold, $P = 0.60$). Although HIF-1α and HIF-2α share similar protein structure and are both key transcriptional regulators of the hypoxic response, several physiological and mechanistic differences between HIF-1α and HIF-2α have been reported [23]. A recent study found a switch in HIF-1α- to HIF-2α-dependent signaling in cancer cells, and that overexpression of the E3-ubiquitin ligase, hypoxia-associated factor, could decrease HIF-1α levels but not HIF-2α in normoxic or hypoxic conditions [24]. Our findings suggest that ARNT2 might be a potential mediator of HIF-1, but not HIF-2, signaling pathways in MCF7 cells; however, the precise mechanism of action remains to be determined.

We observed significant changes to the expressions of several other proteins in response to ARNT2 knockdown, including an increase in SAG expression, and decreases in VHL and MMP1

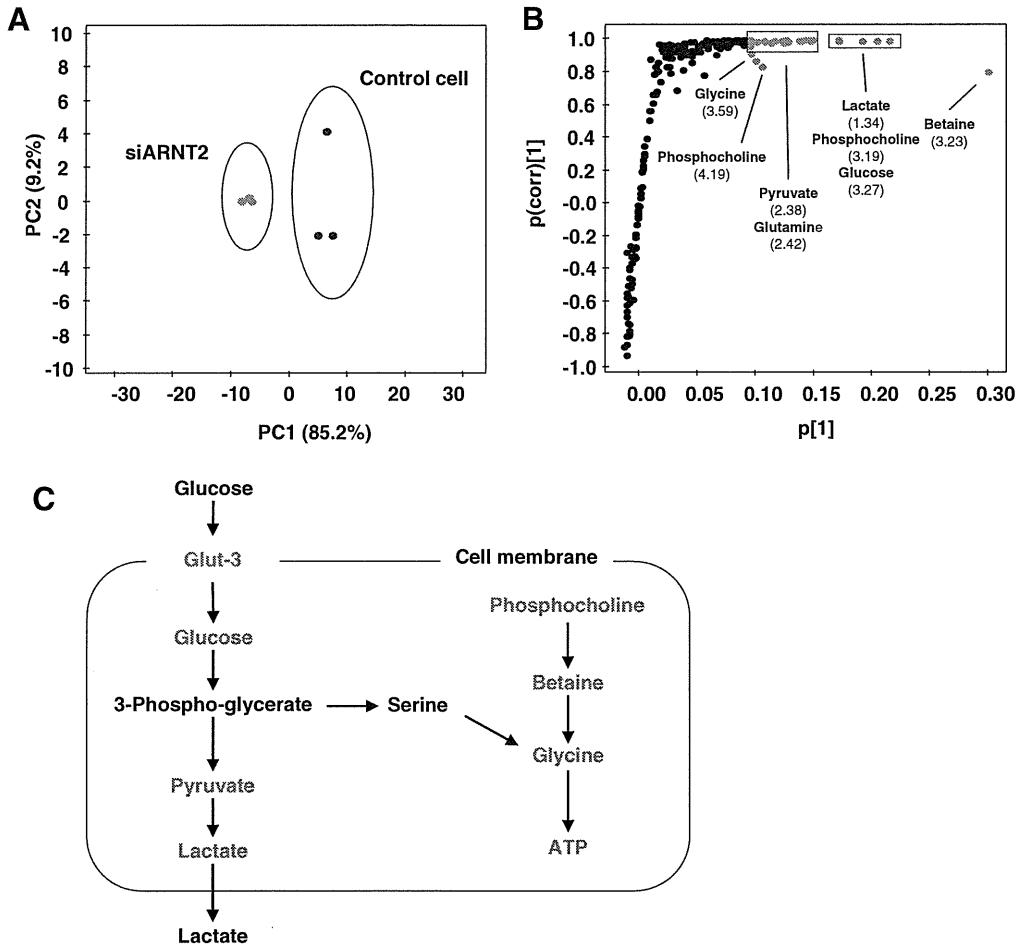

Fig. 4. Statical analysis of metabolites in MCF7 cells. Cells were treated with 10 nM siARNT2 for 72 h and then cultured for another 48 h in steroid-free media without siARNT2 treatment. PCA score plots (A) and OPLS-DA loading S-plots (B) were applied to the intercellular metabolic profiles to assess siARNT2 treatment-related effects. Blue and orange are used to mark control cells and cells treated with siARNT2 in the PCA score plots, respectively. Key metabolites (orange) related with glycine synthesis and glucose metabolism were highlighted in the S-plot. Schematic representation of the metabolic pathways showing the most relevant metabolic changes induced by siARNT2 treatment was summarized according to KEGG metabolism map (C). Blue and green are used to mark downregulated genes and metabolites following siARNT2 treatment, respectively. Metabolites that do not show any significant changes or for which there are no measurements in this study are shown in black.

expressions. VHL is a well-known tumor suppressor, and inactivation of VHL has been implicated in the pathogenesis of several cancers [25]. The cellular levels of HIF-1α are tightly regulated via post-translation modification by prolyl hydroxylases and the VHL, Cullin and Elongin B/C E3-ubiquitin ligase [26]. Furthermore, in renal carcinoma cells, VHL has been shown to negatively regulate HIF-1α and other hypoxia-inducible genes [25,27]. When VHL expression is lost in renal cancers, HIF-1α is constitutively stable (even in normoxia), resulting in constitutive transcription of its target genes and the loss of VHL-mediated tumor suppression. In our study, the knockdown of ARNT2 mRNA expression inhibited VHL expression, which, in turn, activated HIF-1α signaling.

We observed an increase in SAG expression in response to ARNT2 knockdown in MCF7 cells. SAG encodes a redox-inducible and apoptosis-protective antioxidant protein that, when overexpressed, protects mammalian cells from hypoxia-induced apoptosis [26]. A HIF-1-SAG feedback loop has been reported previously, where the inactivation of VHL induces HIF-1 to transactivate SAG, which, in turn, mediates the ubiquitination and degradation of HIF-1α [26]. This feedback loop is in accordance with our observations. In addition, the inhibition of HIF-1α may have caused the decrease in MMP1 that we observed, and potentially other hypoxia-inducible genes [28,29]. It should be noted that the knockdown of ARNT2 expression showed differential effects on the transcriptions of HIF-target genes (as shown in Fig. 2). Although several factors involved in the regulation of gene expression might contribute to this, including differences in the promoter structure and binding affinity, further study is warranted to ascertain the underlying mechanism of action.

Numerous reports have alluded to the shift in glucose metabolism that occurs in cancer cells: from oxidative to glycolytic pathways, in the presence of oxygen [7]. This process is known as the Warburg effect, where HIF-1α-dependent transcriptional regulation of virtually all of the genes in the glycolytic pathways lies at the center of this effect, including the regulation of glucose transporters, glycolytic enzymes, proteins involved in lactate production and others involved in pyruvate metabolism [8]. Our gene expression analysis found that the downregulation of ARNT2 mRNA expression in MCF7 cells significantly inhibited the expression of Glut-3: a predominant glucose transporter responsible for glucose uptake in neurons and cancer cells. This finding indicates that ARNT2 may regulate HIF-1-mediated glucose and energy metabolism [29]. Our metabolite analysis lends further support to this hypothesis, with significant decreases in glycine, an essential precursor of ATP synthesis, as well as other intermediates related to glycine synthesis (phosphocholine and betaine) in cells treated with siARNT2. Moreover, the breakdown products of pyruvate and lactate were also decreased following siARNT2 treatment. Our results suggest that the knockdown of ARNT2 mRNA expression may disrupt HIF-1-regulated glucose and energy metabolism

by inhibiting the expression of hypoxia-inducible genes, such as Glut-3 (Fig. 4C). These observations are in agreement with previous studies, suggesting that disruption of the HIF-1 pathway in tumor cells could impair the supply of anabolic precursors required for cell synthesis [7,21].

In our previous study, we showed that xenoestrogens, such as bisphenol A (BPA), can downregulate ARNT2 mRNA and protein expressions in MCF7 cells [15]. Combined with these new findings, it is plausible to suggest that prenatal and/or long-term chronic exposure to xenoestrogens could affect human fetal health by impairing ARNT2 function, without any significant symptoms, until the accumulated effects possibly lead to tumorigenesis in later life. This may be of particular importance because humans are still widely exposed to xenoestrogens. For example, BPA is still produced worldwide and employed in the manufacture of commonly used polycarbonate plastic products and personal care products [30].

ARNT2 is involved in numerous other physiological pathways, such as in AHR signaling, which is important in the metabolic activation and detoxification of ubiquitous environmental pollutants and carcinogens, including dioxins and benzo[*a*]pyrenes (BaP) [1–3]. Interestingly, a recent study reported a two-way interaction between HIF-1 and AHR pathways, where HIF-1α activation significantly reduced the levels of AHR downstream targets genes and increased BaP-induced genetic instability [31]. Our results suggest that ARNT2 may play a role in cancer development by a HIF-1-mediated mechanism that perhaps also includes the modulation of AHR signaling and carcinogen metabolism. However, the details of this mechanism of action are still unclear, and further experimentation is warranted.

5. Conclusions

In summary, we described a role for ARNT2 in the modulation of HIF-1-regulated signaling and metabolism in MCF7 cells. ARNT2 is an essential regulator involved in the physiological response to several critical environmental insults, including chemical toxins and hypoxia. The regulatory effects of ARNT2 on the tumor suppressor activity of VHL and the anti-apoptosis activity of SAG suggest the potential role of ARNT2 in cancer development, treatment and outcome. However, a detailed mechanism of action is still unclear from this limited study, and further research to elucidate the functions of ARNT2 in more detail is necessary in epidemiology studies and in different in vivo and in vitro models.

Acknowledgment

This study was supported in part by the Environmental Technology Development Fund from the Ministry of the Environment, Japan.

References

[1] Hirose, K., Morita, M., Ema, M., Mimura, J., Hamada, H., Fujii, H., Saijo, Y., Gotoh, O., Sogawa, K. and Fujii-Kuriyama, Y. (1996) CDNA cloning and tissue-specific expression of a novel basic helix-loop-helix/PAS factor (Arnt2) with close sequence similarity to the aryl hydrocarbon receptor nuclear translocator (Arnt). Mol. Cell. Biol. 16, 1706–1713.
[2] Sekine, H., Mimura, J., Yamamoto, M. and Fujii-Kuriyama, Y. (2006) Unique and overlapping transcriptional roles of arylhydrocarbon receptor nuclear translocator (Arnt) and Arnt2 in xenobiotic and hypoxic responses. J. Biol. Chem. 281, 37507–37516.
[3] Hankinson, O. (2008) Why does ARNT2 behave differently from ARNT? Toxicol. Sci. 103, 1–3.
[4] Maltepe, E., Keith, B., Arsham, A.M., Brorson, J.R. and Simon, M.C. (2000) The role of ARNT2 in tumor angiogenesis and the neural response to hypoxia. Biochem. Biophys. Res. Commun. 273, 231–238.
[5] Martinez, V., Kennedy, S., Doolan, P., Gammell, P., Joyce, H., Kenny, E., Prakash Mehta, J., Ryan, E., O'Connor, R., Crown, J., Clynes, M. and O'Driscoll, L. (2008) Drug metabolism-related genes as potential biomarkers: analysis of expression in normal and tumour breast tissue. Breast Cancer Res. Treat. 110, 521–530.
[6] Fiehn, O. (2002) Metabolomics—the link between genotypes and phenotypes. Plant Mol. Biol. 48, 155–171.
[7] Denko, N.C. (2008) Hypoxia, HIF1 and glucose metabolism in the solid tumour. Nat. Rev. Cancer 8, 705–713.
[8] Rankin, E.B. and Giaccia, A.J. (2008) The role of hypoxia-inducible factors in tumorigenesis. Cell Death Differ. 15, 678–685.
[9] Reo, N.V. (2002) NMR-based metabolomics. Drug Chem. Toxicol. 25, 375–382.
[10] Coen, M., Holmes, E., Lindon, J.C. and Nicholson, J.K. (2008) NMR-based metabolic profiling and metabonomic approaches to problems in molecular toxicology. Chem. Res. Toxicol. 21, 9–27.
[11] Weljie, A.M., Bondareva, A., Zang, P. and Jirik, F.R. (2011) ^{1}H NMR metabolomics identification of markers of hypoxia-induced metabolic shifts in a breast cancer model system. J. Biomol. NMR 49, 185–193.
[12] Cano, K.E., Li, Y.J. and Chen, Y. (2010) NMR metabolomic profiling reveals new roles of SUMOylation in DNA damage response. J. Proteome Res. 9, 5382–5388.
[13] Ellis, J.K., Athersuch, T.J., Cavill, R., Radford, R., Slattery, C., Jennings, P., McMorrow, T., Ryan, M.P., Ebbels, T.M. and Keun, H.C. (2011) Metabolic response to low-level toxicant exposure in a novel renal tubule epithelial cell system. Mol. BioSyst. 7, 247–257.
[14] Griffin, J.L. (2003) Metabonomics: NMR spectroscopy and pattern recognition analysis of body fluids and tissues for characterisation of xenobiotic toxicity and disease diagnosis. Curr. Opin. Chem. Biol. 7, 648–654.
[15] Qin, X.Y., Zaha, H., Nagano, R., Yoshinaga, J., Yonemoto, J. and Sone, H. (2011) Xenoestrogens down-regulate aryl-hydrocarbon receptor nuclear translocator 2 mRNA expression in human breast cancer cells via an estrogen receptor alpha-dependent mechanism. Toxicol. Lett. 206, 152–157.
[16] Sheikh, K.D., Khanna, S., Byers, S.W., Fornace Jr., A. and Cheema, A.K. (2011) Small molecule metabolite extraction strategy for improving LC/MS detection of cancer cell metabolome. J. Biomol. Tech. 22, 1–4.
[17] Wei, F., Furihata, K., Hu, F., Miyakawa, T. and Tanokura, M. (2010) Complex mixture analysis of organic compounds in green coffee bean extract by two-dimensional NMR spectroscopy. Mag. Res. Chem. 48, 857–865.
[18] Hosoya, T., Oda, Y., Takahashi, S., Morita, M., Kawauchi, S., Ema, M., Yamamoto, M. and Fujii-Kuriyama, Y. (2001) Defective development of secretory neurones in the hypothalamus of Arnt2-knockout mice. Genes Cells 6, 361–374.
[19] Hsu, H.J., Wang, W.D. and Hu, C.H. (2001) Ectopic expression of negative ARNT2 factor disrupts fish development. Biochem. Biophys. Res. Commun. 282, 487–492.
[20] Harris, A.L. (2002) Hypoxia—a key regulatory factor in tumour growth. Nat. Rev. Cancer 2, 38–47.
[21] Griffiths, J.R., McSheehy, P.M., Robinson, S.P., Troy, H., Chung, Y.L., Leek, R.D., Williams, K.J., Stratford, I.J., Harris, A.L. and Stubbs, M. (2002) Metabolic changes detected by in vivo magnetic resonance studies of HEPA-1 wild-type tumors and tumors deficient in hypoxia-inducible factor-1beta (HIF-1beta): evidence of an anabolic role for the HIF-1 pathway. Cancer Res. 62, 688–695.
[22] Carroll, V.A. and Ashcroft, M. (2006) Role of hypoxia-inducible factor (HIF)-1alpha versus HIF-2alpha in the regulation of HIF target genes in response to hypoxia, insulin-like growth factor-I, or loss of von Hippel-Lindau function: implications for targeting the HIF pathway. Cancer Res. 66, 6264–6270.
[23] Bracken, C.P., Fedele, A.O., Linke, S., Balrak, W., Lisy, K., Whitelaw, M.L. and Peet, D.J. (2006) Cell-specific regulation of hypoxia-inducible factor (HIF)-1α and HIF-2α stabilization and transactivation in a graded oxygen environment. J. Biol. Chem. 281, 22575–22585.
[24] Koh Jr., M.Y., Lemos, R., Liu, X. and Powis, G. (2011) The hypoxia-associated factor switches cells from HIF-1α- to HIF-2α-dependent signaling promoting stem cell characteristics, aggressive tumor growth and invasion. Cancer Res. 71, 4015–4027.
[25] Iliopoulos, O., Levy, A.P., Jiang, C., Kaelin Jr., W.G. and Goldberg, M.A. (1996) Negative regulation of hypoxia-inducible genes by the von Hippel-Lindau protein. Proc. Natl. Acad. Sci. USA 93, 10595–10599.
[26] Tan, M., Gu, Q., He, H., Pamarthy, D., Semenza, G.L. and Sun, Y. (2008) SAG/ROC2/RBX2 is a HIF-1 target gene that promotes HIF-1 alpha ubiquitination and degradation. Oncogene 27, 1404–1411.
[27] Baldewijns, M.M., van Vlodrop, I.J., Vermeulen, P.B., Soetekouw, P.M., van Engeland, M. and de Bruine, A.P. (2010) VHL and HIF signalling in renal cell carcinogenesis. J. Pathol. 221, 125–138.
[28] Sun, X., Wei, L., Chen, Q. and Terek, R.M. (2010) CXCR4/SDF1 mediate hypoxia induced chondrosarcoma cell invasion through ERK signaling and increased MMP1 expression. Mol. Cancer 9, 17.
[29] Liu, Y., Liu, F., Iqbal, K., Grundke-Iqbal, I. and Gong, C.X. (2008) Decreased glucose transporters correlate to abnormal hyperphosphorylation of tau in Alzheimer disease. FEBS Lett. 582, 359–364.
[30] Vandenberg, L.N., Hauser, R., Marcus, M., Olea, N. and Welshons, W.V. (2007) Human exposure to bisphenol A (BPA). Reprod. Toxicol. 24, 139–177.
[31] Schults, M.A., Timmermans, L., Godschalk, R.W., Theys, J., Wouters, B.G., van Schooten, F.J. and Chiu, R.K. (2010) Diminished carcinogen detoxification is a novel mechanism for hypoxia-inducible factor 1-mediated genetic instability. J. Biol. Chem. 285, 14558–14564.

Toxicology Letters 206 (2011) 152–157

Contents lists available at ScienceDirect

Toxicology Letters

journal homepage: www.elsevier.com/locate/toxlet

Xenoestrogens down-regulate aryl-hydrocarbon receptor nuclear translocator 2 mRNA expression in human breast cancer cells via an estrogen receptor alpha-dependent mechanism

Xian-Yang Qin[a,b], Hiroko Zaha[a], Reiko Nagano[a], Jun Yoshinaga[b], Junzo Yonemoto[a], Hideko Sone[a,*]

[a] Research Center for Environmental Risk, National Institute for Environmental Studies, 16-2 Onogawa, Tsukuba 305-8506, Japan
[b] Department of Environmental Studies, The University of Tokyo, Kashiwanoha 5-1-5, Kashiwa, Chiba 270-8563, Japan

ARTICLE INFO

Article history:
Received 20 January 2011
Received in revised form 1 July 2011
Accepted 4 July 2011
Available online 12 July 2011

Keywords:
ARNT2
Xenoestrogen
E-CALUX
Endocrine disruption
Tumorigenesis

ABSTRACT

Environmental chemicals with estrogenic activity, known as xenoestrogens, may cause impaired reproductive development and endocrine-related cancers in humans by disrupting endocrine functions. Aryl-hydrocarbon receptor nuclear translocator 2 (ARNT2) is believed to play important roles in a variety of physiological processes, including estrogen signaling pathways, that may be involved in the pathogenesis and therapeutic responses of endocrine-related cancers. However, much of the underlying mechanism remains unknown. In this study, we investigated whether ARNT2 expression is regulated by a range of representative xenoestrogens in human cancer cell lines. Bisphenol A (BPA), benzyl butyl phthalate (BBP), and 1,1,1-trichloro-2,2-bis(2-chlorophenyl-4-chlorophenyl)ethane (*o,p'*-DDT) were found to be estrogenic toward BG1Luc4E2 cells by an E-CALUX bioassay. ARNT2 expression was downregulated by BPA, BBP, and *o,p'*-DDT in a dose-dependent manner in estrogen receptor 1 (ESR1)-positive MCF-7 and BG1Luc4E2 cells, but not in estrogen receptor-negative LNCaP cells. The reduction in ARNT2 expression in cells treated with the xenoestrogens was fully recovered by the addition of a specific ESR1 antagonist, MPP. In conclusion, we have shown for the first time that ARNT2 expression is modulated by xenoestrogens by an ESR1-dependent mechanism in MCF-7 breast cancer cells.

1. Introduction

Environmental chemicals with estrogenic activity, known as xenoestrogens, are currently the largest group of known endocrine disruptors (EDs) (Welshons et al., 2003). Over the past few decades, a considerable number of publications have indicated that maternal exposure to EDs may cause impaired reproductive development and endocrine-related cancers in humans by disrupting endocrine functions. Concerns have been focused on a variety of environmental chemicals, including bisphenol A (BPA), phthalates, organochlorine pesticides, dioxin and polychlorinated biphenyls and their hydroxylated metabolites (OH-PCBs). However, the findings remain controversial (Safe, 2004; Sharpe and Irvine, 2004; Sikka and Wang, 2008). An excellent example of an ED is diethylstilbestrol (DES), a synthetic estrogen that was administered to pregnant women to prevent miscarriage during the 1940s and 1970s. It is currently well understood that prenatal exposure to DES may be associated with adverse pregnancy outcomes, genital tract abnormalities, infertility, and vaginal and cervical cancers (Hatch et al., 2010; Ma, 2009).

Aryl-hydrocarbon receptor nuclear translocator 2 (ARNT2) is a member of the basic helix-loop-helix Per-ARNT-SIM (bHLH-PAS) family of transcription factors (Hirose et al., 1996) and acts as a common obligate partner for several other members of the family, including aryl hydrocarbon receptor (AHR) and hypoxia-inducible factor (HIF)-1α (Hankinson, 2008; Sekine et al., 2006). ARNT2 knockout mice suffer severe developmental defects and die shortly after birth (Hosoya et al., 2001). Similar findings were observed in the zebrafish (Hsu et al., 2001). Although many of the functions of ARNT2 remain unknown, it is believed that ARTN2 may play important roles in tumor angiogenesis (Maltepe et al., 2000) and many physiological pathways, including the responses to environmental contaminants, oxygen deprivation, biological rhythms, angiogenesis, and neuronal development (Hill et al., 2009). In addition, a recent epidemiological study found that ARNT2 expression was correlated with the prognosis of breast cancer patients by participating in the metabolism of certain environmental chemicals, indicating potential interactions between ARNT2 and estrogen receptor (ER) signaling pathways (Martinez et al., 2008).

In this study, we investigated the effects of xenoestrogens on ARNT2 expression in two estrogen-dependent cancer cell lines,

* Corresponding author. Tel.: +81 29 850 2546; fax: +81 29 850 2546.
E-mail address: hsone@nies.go.jp (H. Sone).

0378-4274/$ – see front matter © 2011 Elsevier Ireland Ltd. All rights reserved.
doi:10.1016/j.toxlet.2011.07.007

MCF-7 human breast cancer cells and BG1Luc4E2 human ovarian cancer cells, and one estrogen-independent cancer cell line, LNCaP human prostate cancer cells. The estrogenic activities of a range of representative EDs were measured using an estrogenic chemically activated luciferase gene expression (E-CALUX) bioassay. We also examined the mechanism of ARNT2 regulation, in terms of the ER-dependent activation pathway.

2. Materials and methods

2.1. Chemicals

Dimethyl sulfoxide (DMSO) and 17β-estradiol (E2) were obtained from Sigma Chemical Co. (St. Louis, MO). 1,3-Bis(4-hydroxyphenyl)-4-methyl-5-[4-(2-piperidinylethoxy)phenol]-1H-pyrazole dihydrochloride (MPP) was obtained from Tocris (Ellisville, MO). DMSO was used as the primary solvent for all chemicals, and the DMSO solutions were further diluted in cell culture media for treatments. The final concentrations of DMSO in the media did not exceed 0.1% (vol/vol).

BPA, benzyl butyl phthalate (BBP), di-*n*-butyl phthalate (DBP), and di(2-ethylhexyl) phthalate (DEHP) were obtained from Wako Industries (Osaka, Japan). 2,3,3′,4′,5-Pentachloro-4-biphenylol (OH-PCB 107), 2,2′,3,4′,5,5′-hexachloro-4-biphenylol (OH-PCB 146), and 2,2′,3,4′,5,5′,6-heptachloro-4-biphenylol (OH-PCB 187) were obtained from Wellington Laboratories (Guelph, ON, Canada). 2,3,7,8-Tetrachlorodibenzo-*p*-dioxin (TCDD) was obtained from Cambridge Isotope Laboratories (Cambridge, MA). 1,1,1-Trichloro-2,2-bis(4-chlorophenyl)ethane (*p,p′*-DDT) and 1,1,1-trichloro-2,2-bis(2-chlorophenyl-4-chlorophenyl)ethane (*o,p′*-DDT) were obtained from AccuStandard (New Haven, CT).

2.2. Cell culture

MCF-7 and LNCaP cells were obtained from the Cell Engineering Division of RIKEN BioResource Center (Tsukuba, Ibaraki, Japan). The BG1Luc4E2 cells used in the E-CALUX bioassay were a gift from Dr. M. Denison (University of California, Davis, CA). The estrogen receptor 1 (ESR1)-positive BG1Luc4E2 cells are BG-1 ovarian cancer cells stably transfected with a luciferase reporter gene under the control of estrogen response element (ERE) that is responsive to the exposure to estrogen or estrogenic chemicals (Rogers and Denison, 2000). MCF-7, LNCaP, and BG1Luc4E2 cells were maintained in RPMI 1640 medium (Wako, Osaka, Japan) containing 10%, 10%, and 8% fetal bovine serum (FBS) (Mediatech, Herndon, VA), respectively. All of the cells were grown at 37 °C in a 5% CO_2 humidified incubator. For growth under steroid-free conditions, the cells were seeded in phenol red-free DMEM (MP Biomedicals, Solon, OH) containing 5% charcoal/dextran-treated FBS (Hyclone, Logan, UT). All the culture media contained 100 U/ml penicillin/streptomycin and 2 mmol/L L-glutamine (Mediatech, Herndon, VA).

2.3. Luciferase assay

BG1Luc4E2 cells were plated in 96-well plates (4×10^4 cells/well) and cultured under steroid-free conditions for 24 h, before exposure to EDs for 24 h. After removal of the medium, the plates were rinsed with phosphate-buffered saline (Gibco, Grand Island, NY), and the cells were lysed with 20 μl/well lysis buffer (Promega, Madison, WI). The luciferase activity was measured in an AB-2100 luminometer (Atto, Tokyo, Japan) after the addition of 100 μl/well luciferase assay reagent (Promega) and expressed as relative light units. Luciferase induction was calculated as a percentage of the vehicle control by setting the induction by DMSO at 100%. The half-maximal effective concentration, EC_{50}, was calculated for each test compound using a previously described method (Alexander et al., 1999).

2.4. Quantitative real-time reverse transcription-polymerase chain reaction (RT-PCR)

Total RNA for real-time RT-PCR was isolated from the three cell lines after treatment with the EDs for 24 h using an RNeasy Kit (Qiagen, Valencia, CA) in accordance with the manufacturer's instructions. Quantification and quality assessment of the isolated RNA samples were performed and verified using an Agilent Bioanalyzer 2100 and an RNA 6000 Nano Assay (Agilent Technologies, Palo Alto, CA) in accordance with the manufacturer's instructions. RNA (9 μg) was transcribed using a High Capacity RNA-to-cDNA Kit (Applied Biosystems, Foster City, CA) according to the manufacturer's instructions. The resulting cDNA (1 μl) was amplified in triplicate using TaqMan® Gene Expression Master Mix (Applied Biosystems) in accordance with the manufacturer's instructions. TaqMan® Gene Expression Assays (Applied Biosystems) used in this study were Hs00208298_m1 for *ARNT2*, Hs00420042_m1 for PDZ domain containing 1 (*PDZK1*), and Hs00266705_g1 for glyceraldehyde-3-phosphate dehydrogenase (*GAPDH*). The amplification reaction was performed in an ABI PRISM 7000 Sequence Detector (Applied Biosystems) under the following cycling conditions: 95 °C for 15 min, followed by 40 cycles of 95 °C for 15 s and 60 °C for 60 s. The gene expression levels were calculated based on the threshold cycle using Sequence Detection System Software (Applied Biosystems). The gene expression was normalized by the GAPDH expression and set to 1 for the control DMSO-treated cells.

2.5. Western blot analysis

To evaluate the effects of EDs exposure on ARNT2 protein expression, Western blot was performed using the polyclonal anti-ARNT2 M-165 antibody from Santa Cruz Biotechnology (sc-5581, 1:500 dilution, Santa Cruz, CA). MCF-7 cells (2.5×10^6) treated with EDs were lysed using RIPA buffer solution (Santa Cruz Biotechnology). After boiling at 99 °C for 5 min, the protein samples were resolved by SDS polyacrylamide gel electrophoresis on a 10% gel and transferred to a polyvinylidene difluoride membrane (Bio-Rad Laboratories, Hercules, CA). After blotting in TBS with 5% nonfat dry milk–Tris buffered saline and 0.1% Tween, the membrane was probed with Actin H-196 (sc-7210, 1:500 dilution, Santa Cruz Biotechnology) or ARNT2 M-165 primary antibody. Blots were then incubated with a horseradish peroxidase (HRP)-conjugated anti-rabbit secondary antibody (ECL plus Western blotting reagent pack, RPN2124, 1:10,000 dilution, GE Healthcare UK, Buckingham, England). The immune complex was detected with the Amersham ECL Plus™ Western Blotting Detection System (RPN2132, GE Healthcare UK). The blots were exposed to Hyperfilm (Amersham Pharmacia Biotech), and bands were quantified with ImageJ densitometry software (National Institutes of Health, Bethesda, MD).

2.6. Statistical analysis

All experiments in this study were performed in triplicates to test the reproducibility of the results. Quantitative data were expressed as the means ± SD. The statistical significance of differences between values was assessed using a two-tailed Student's *t*-test. Values of $P < 0.05$ were considered to indicate statistical significance.

3. Results

3.1. Estrogenic activities of EDs toward BG1Luc4E2 cells

The effects of E2 and several EDs on ESR1-mediated luciferase induction were measured by an E-CALUX bioassay in the human ovarian cancer cell line BG1Luc4E2 (Fig. 1 and Table 1). E2 significantly increased the ESR1-induced luciferase activity in a dose-dependent manner compared with the control DMSO-treated

Table 1
Estrogenic activity of EDs in the E-CALUX bioassay.

Chemicals	LOEC (M)	EC_{50} (M)	MOEC (M)	% of control (max)
E2	4.1×10^{-13}	4.8×10^{-13}	1×10^{-10}	263
BPA	1.23×10^{-7}	2×10^{-7}	3.33×10^{-6}	220
BBP	1.23×10^{-7}	2.45×10^{-7}	1×10^{-5}	295
DBP	–	–	–	–
DEHP	–	–	–	–
o,p′-DDT	3.13×10^{-7}	8.92×10^{-7}	5×10^{-6}	285
p,p′-DDT	3.13×10^{-7}	nd	5×10^{-6}	175
OH-PCB107	1.4×10^{-7}	nd	1.4×10^{-7}	117
OH-PCB146	2.3×10^{-10}	nd	1.3×10^{-7}	122
OH-PCB187	4.8×10^{-8}	nd	2.4×10^{-8}	125
TCDD	4.96×10^{-11}	6.0×10^{-10}	1.55×10^{-7}	43

LOEC, lowest observed effect concentration; EC_{50}, half of maximum effect concentration; MOEC, maximum observed effect concentration; –, no effect observed; nd, not determined; M, mol/L.

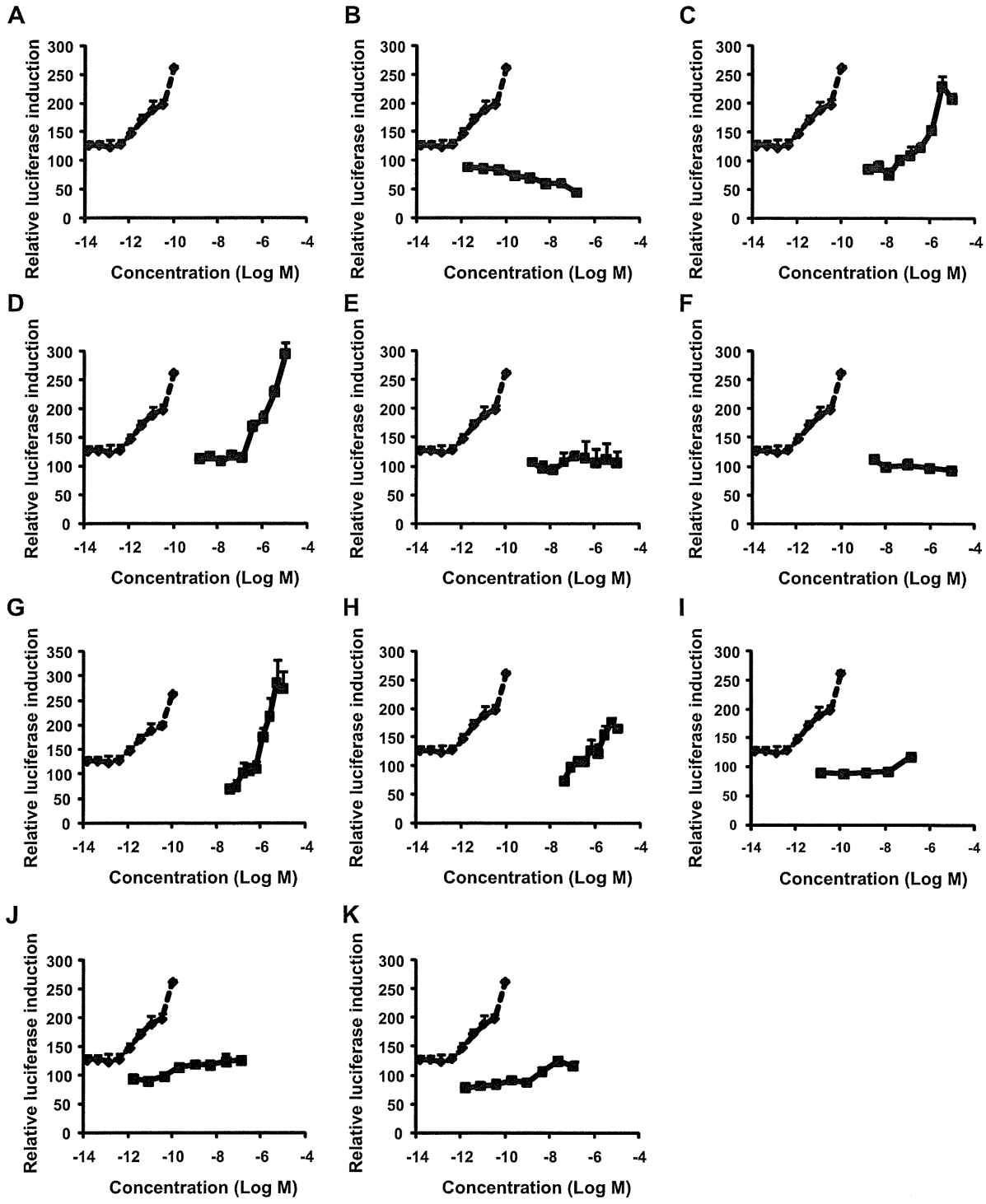

Fig. 1. Effects of xenoestrogens on the induction of ESR1-induced luciferase activity in the E-CALUX bioassay. BG1Luc4E2 cells were treated with E2 (A), TCDD (B), BPA (C), BBP (D), DBP (E), DEHP (F), *o,p′*-DDT (G), *p,p′*-DDT (H), OH-PCB107 (I), OH-PCB146 (J), and OH-PCB187 (K) at increasing concentrations for 24 h. All the data are expressed as the percentage of the vehicle control (DMSO) treatment. Each value is the mean ± SD of a representative experiment performed in triplicate. The data for E2 (dotted lines) are shown in all the compound charts for comparison.

cells, with maximal stimulation at 10^{-10} M. Among the EDs, BPA, BBP, and *o,p′*-DDT increased the ESR1-induced luciferase activity in a dose-dependent manner at 10^{-7} M to 10^{-5} M for BPA and *o,p′*-DDT, and at 10^{-8} M to 10^{-5} M for BBP. Weak, but significant, effects were observed for *p,p′*-DDT and OH-PCB107 at 10^{-5} M and 10^{-7} M, respectively. No significant effects were observed for DBP, DEHP, OH-PCB146, or OH-PCB187. TCDD, a well-known AHR ligand, significantly decreased the ESR1-induced luciferase activity in a dose-dependent manner at 5×10^{-11} M to 10^{-7} M. These results suggest that the EDs BPA, BBP, and *o,p′*-DDT may act as ESR1 agonists.

3.2. Modulation of ARNT2 expression by xenoestrogens in MCF-7, BG1Luc4E2, and LNCaP cells

The estrogenic effects of xenoestrogens are primarily mediated by ERs, including ESR1 and estrogen receptor 2 (ESR2) (Watanabe

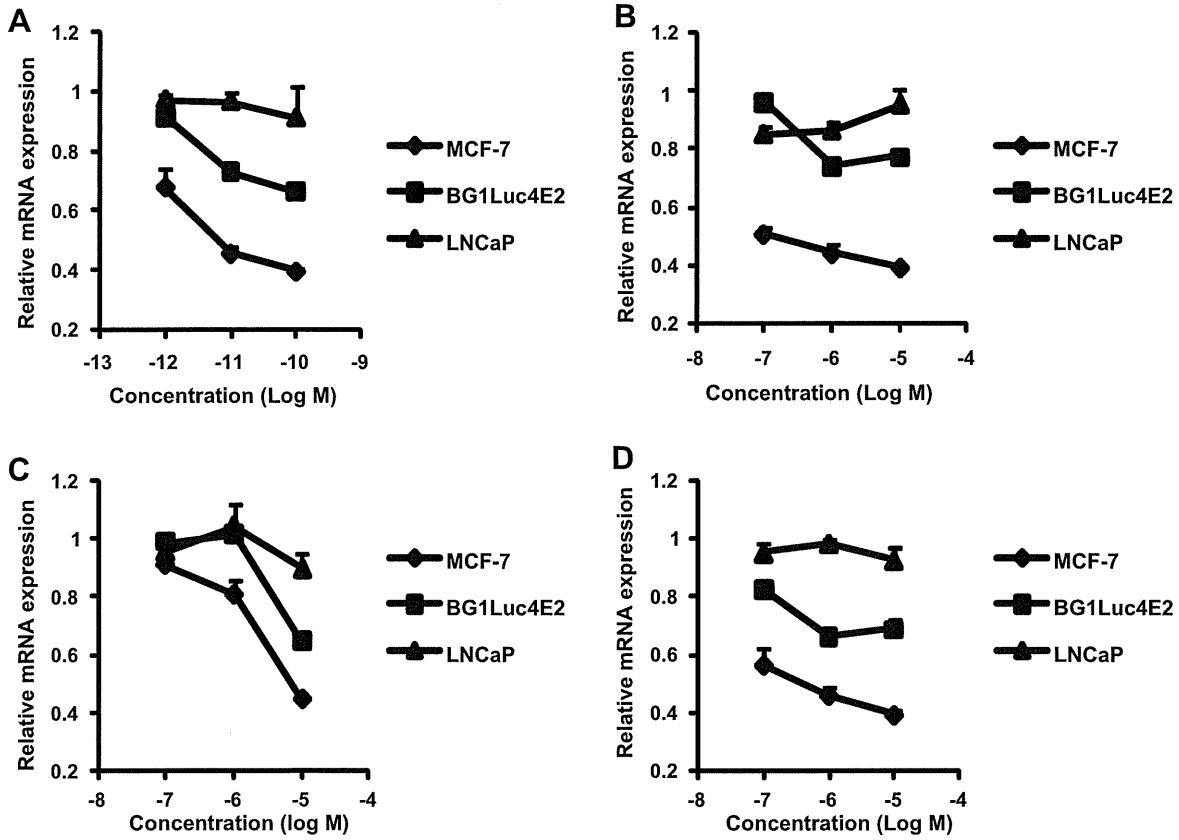

Fig. 2. Modulation of ARNT2 mRNA expression in MCF-7, BG1Luc4E2, and LNCaP cells by xenoestrogens. Cells were treated with DMSO or increasing concentrations of E2 (A), BPA (B), BBP (C), or *o,p′*-DDT (D) for 24 h. All the data are expressed as the fold induction relative to the vehicle control (DMSO) treatment. Each value is the mean ± SD of a representative experiment performed in triplicate.

et al., 2007). Since the presence of these two ER subtypes may contribute to differences in the binding affinities of certain compounds and the subsequent activation of gene expression in various tissues, we examined whether MCF-7, BG1Luc4E2, and LNCaP cells expressed ESR1 and ESR2. The presence of ESR1 mRNA in MCF-7 and BG1Luc4E2 cells and the absence of both ESR1 and ESR2 mRNAs in LNCaP cells were confirmed by real-time RT-PCR (data not shown).

To investigate the abilities of xenoestrogens to modulate ARNT2 expression, MCF-7, BG1Luc4E2, and LNCaP cells were treated for 24 h with E2 and different xenoestrogens at increasing concentrations that induced the minimal, median, and maximal luciferase activities in the E-CALUX bioassay (see Table 1). The expression level of ARNT2 mRNA was determined by quantitative real-time RT-PCR (Fig. 2). E2 and the xenoestrogens BPA, BBP, and *o,p′*-DDT significantly decreased ARNT2 expression in ESR1-positive MCF-7 and BG1Luc4E2 cells in a dose-dependent manner. E2 was able to decrease ARNT2 expression at low concentrations of 10^{-12} to 10^{-10} M (0.39-fold and 0.66-fold reduction at 10^{-10} M in MCF-7 and BG1Luc4E2 cells, respectively; Fig. 2A). Maximal effects were observed at 10^{-5} M for BPA, BBP, and *o,p′*-DDT (0.39-fold and 0.78-fold reduction for BPA, 0.45-fold and 0.65-fold reduction for BBP, and 0.39-fold and 0.69-fold reduction for *o,p′*-DDT in MCF-7 and BG1Luc4E2 cells, respectively; Fig. 2B-D). No significant effects were observed in ER-negative LNCaP cells for any of the chemical compounds (Fig. 2).

We also investigated the effects of E2 and xenoestrogens exposure on ARNT2 protein expression in MCF-7 cells using Western blot analysis. As shown in Fig. 3, significant decreases in ARNT2 protein levels were observed following E2 and xenoestrogens BPA, BBP, and *o,p′*-DDT treatments.

3.3. *The modulation of ARNT2 expression in MCF-7 cells by xenoestrogens is ESR1-dependent*

Next, we investigated whether the xenoestrogens decreased ARNT2 expression in MCF-7 cells in an ESR1-dependent manner.

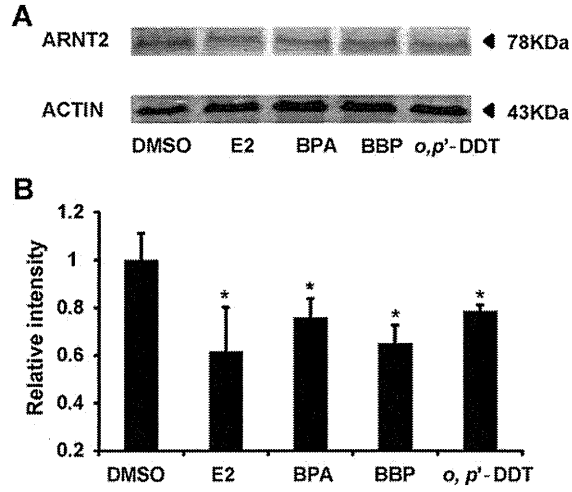

Fig. 3. Modulation of ARNT2 protein expression in MCF-7 cells by xenoestrogens. (A) Cells were treated with DMSO, 0.1 nM E2, 10 μM BPA, 10 μM BBP, or 10 μM *o,p′*-DDT for 24 h, and then analyzed by Western blot. (B) The cellular protein levels of ARNT2 were calculated using ImageJ densitometry software and are expressed as the mean ± SD relative to vehicle control (DMSO) after normalizing the bands to ACTIN. Representative data were shown from triplicate experiments. *$P < 0.05$ vs. the vehicle control (DMSO).

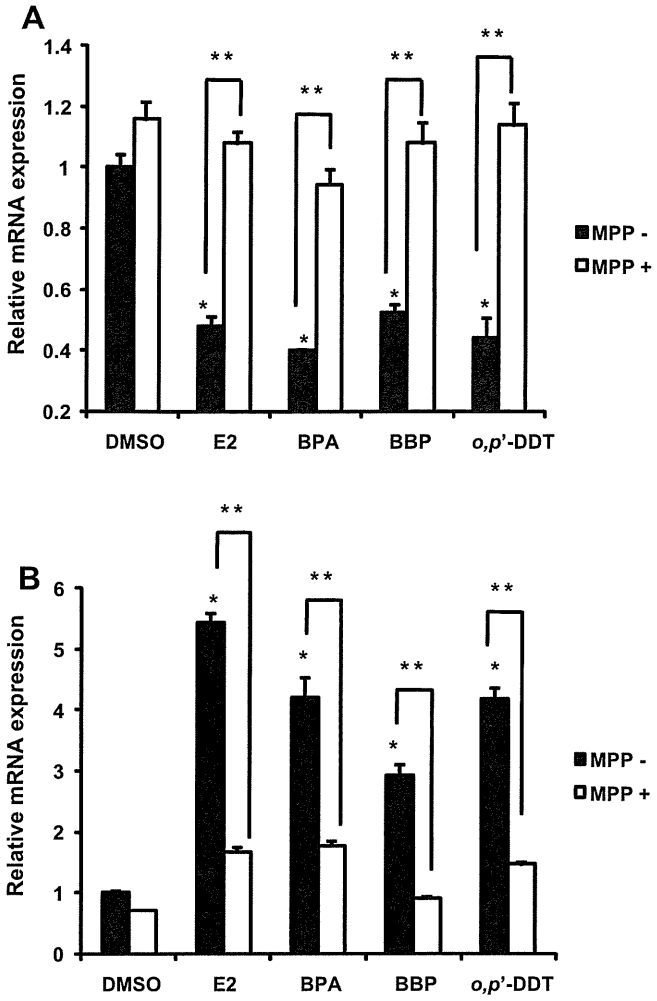

Fig. 4. ARNT2 mRNA expression decrease mediated by xenoestrogens is increased by MPP in breast cancer cells. MPP, an ESR1 antagonist, blocks the ability of xenoestrogens to modulate ARNT2 (A) and PDZK1 (B) expression in MCF-7 cells. Cells were treated with DMSO, 0.1 nM E2, 10 μM BPA, 10 μM BBP, or 10 μM *o,p'*-DDT for 24 h alone or in combination with 0.1 μM MPP. All the data are expressed as the fold induction relative to the vehicle control (DMSO) treatment. Each value is the mean ± SD of a representative experiment performed in triplicate. *$P < 0.05$ vs. the vehicle control, **$P < 0.05$ vs. the corresponding xenoestrogen control.

To achieve this, we examined the effects of the specific ESR1 antagonist MPP, which has been shown to selectively block ESR1- but not ESR2-mediated transactivation (Harrington et al., 2003). As shown in Fig. 4A, the decrease in ARNT2 expression was significantly inhibited in MCF-7 cells after the addition of MPP in the presence of E2, BPA, BBP, and *o,p'*-DDT. PDZK1, a well-known estrogen-regulated gene expressed in hormone-responsive breast cancer (Ghosh et al., 2000), was used as a positive control in this experiment. As shown in Fig. 4B, E2 at 10^{-10} M, and BPA, BBP, and *o,p'*-DDT at 10^{-5} M significantly increased PDZK1 expression (5.4-fold, 4.2-fold, 2.9-fold, and 4.2-fold induction, respectively). The levels of PDZK1 mRNA after stimulation with E2 and xenoestrogens were fully recovered in the presence of the specific ESR1 antagonist MPP. Taken together, these findings indicate that the modulatory effects of xenoestrogens on ARNT2 expression are dependent on ESR1-mediated pathways.

4. Discussion

In this present study, we have shown that xenoestrogens significantly decrease ARNT2 expression in MCF-7 breast cancer cells through an ESR1-dependent pathway. We determined the estrogenic and anti-estrogenic activities of a variety of EDs, including BPA, BBP, *o,p'*-DDT, and TCDD in BG1Luc4E2 ovarian cancer cells by an ERE-luciferase bioassay. Our results are consistent with previous reports in other human cell lines, although the approaches applied for the estrogenic activity measurements differed slightly (Buteau-Lozano et al., 2008; Ghisari and Bonefeld-Jorgensen, 2009; Rogers and Denison, 2002). The previous report that BG1Luc4E2 cells are positive for ESR1 but not ESR2 indicates that these chemicals mediate the expression of the ERE-luciferase gene by ESR1-mediated pathways (Rogers and Denison, 2000). Our findings that xenoestrogens such as BPA, BBP, and *o,p'*-DDT downregulated ARNT2 expression in ESR1-positive MCF-7 and BG1Luc4E2 cells but not in ER-negative LNCaP cells suggest ESR1 may play an important role in the mechanism by which xenoestrogens exert their effects on ARNT2 expression. This notion is further confirmed by the significant inhibition of the xenoestrogen-mediated decrease in ARNT2 expression in MCF-7 cells after the addition of the specific ESR1 antagonist MPP.

Recent research has focused on the roles of ARNT2 in a variety of physiological processes, such as AHR, HIF-1α, and ER signaling pathways, that may be involved in the pathogenesis and therapeutic responses of endocrine-related cancers (Hankinson, 2008; Swedenborg and Pongratz, 2010). However, only two animal studies have attempted to determine the potential effects of E2 on ARNT2 expression in rat models, and their conclusions differed. Mitsushima et al. (2003) described that a subcutaneous injection of E2 increased the expression of Arnt2 mRNA in the mediobasal hypothalamus of ovariectomized rats, while no effects were observed in the preoptic area. In contrast, Kretzschmar et al. (2010) observed downregulation of Arnt2 mRNA expression following a subcutaneous injection of E2 in a dose-dependent manner in the uterus of ovariectomized rats. Although neither of the above-said two studies investigated the underlying mechanism, the differing distributions of the two ER subtypes (ESR1 and ESR2) may account for the different regulations of ARNT2 expression by E2. The presence and relative amounts of each ER subtype may contribute to the differential effects of certain ligands in various tissues, since ESR1 and ESR2 are known to show differences in their relative binding affinities for particular compounds and the subsequent activation of gene expression (Heldring et al., 2007; Kuiper et al., 1997). Our present study provided another evidence that E2 and xenoestrogens might down-regulate ARNT2 mRNA expression in cultured cells. We confirmed the high expression of ESR1 and low expression of ESR2 in human ovarian and breast cancer cells. These results are consistent with previous reports indicating that the ratio of ESR1 to ESR2 (which is normally around one) is altered when ovarian and breast tissues or cells become cancerous, such that ESR1 becomes predominant and ESR2 is dramatically decreased (Brandenberger et al., 1998; Hevir et al., 2011). Furthermore, we found that the suppression of ARNT2 expression after E2 and xenoestrogen treatment was completely reversed in the presence of the specific ESR1 antagonist MPP. Our findings suggest that ESR1-mediated pathways may play principal roles in both ARNT2 expression regulation and the estrogenic activities of xenoestrogens.

To the best of our knowledge, this is the first report that the expression of ARNT2 mRNA is regulated by xenoestrogens in human ESR1-positive cancer cell lines. This may be of particular interest because ARNT2 mRNA expression was reported to be much more prevalent in tumor tissues than in normal tissues and to be significantly correlated with a better prognosis of breast cancer patients (Martinez et al., 2008). An important problem in the treatment of breast cancer patients is that long-term anti-estrogen therapy may result in tumor progression to an estrogen-independent stage and loss of drug sensitivity. Hypoxia is

supposed to be one of the possible factors that promote estrogen-independent growth of breast cancer cells (Scherbakov et al., 2009). ARNT2 protein dimerizes with HIF-1α, and the heterodimer then binds to hypoxia-responsive elements in a variety of responsive genes. These genes may play integral roles in the body's response to low oxygen concentrations or hypoxia and a number of pathological conditions including cancer, heart disease, cerebrovascular disease, and chronic obstructive pulmonary disease (Maltepe et al., 2000; Sekine et al., 2006; Ziello et al., 2007). Our present findings suggest a possible mechanism that downregulation of ARNT2 expression by xenoestrogens may result in the progression of tumors by affecting HIF-1α pathways and endocrine responsiveness and resistance. ARNT2 protein is also assumed to dimerize with AHR, an essential transcription factor in physiologic responses to ubiquitous environmental pollutants and carcinogens that plays an important role in mammary gland tumorigenesis (Schlezinger et al., 2006; Sekine et al., 2006). Our recent findings also indicate a possible mechanism that xenoestrogens may have profound consequences on AHR-mediated detoxification by mediating ARNT2 expression. However, the issue of whether ARTN2 participates in AHR pathways remains controversial (Dougherty and Pollenz, 2008; Hankinson, 2008).

In summary, we have described for the first time that ARNT2 expression is modulated by xenoestrogens in MCF-7 breast cancer cells, in parallel with their estrogenic activity mediated by ESR1 pathways. ARNT2 is believed to be an essential participant in the physiologic responses to many important environmental insults, including chemical toxicants and hypoxia (Hankinson, 2008). The wide exposure to xenoestrogens requires further research to elucidate the functions of the ARNT2 protein in different in vivo and in vitro models in more detail.

Conflict of interest statement

The authors declare that they have no financial or non-financial competing interests.

Acknowledgments

This research was supported by a Grant-in-Aid for Scientific Research from the Ministry of Health, Labour and Welfare of Japan. This research was also partly supported by the Environment Research and Technology Development Fund (C-0905) of the Ministry of the Environment, Japan. We thank Mr. Masafumi Nakamura and Mr. Hiroshi Handa (Hiyoshi Corporation, Omihachiman, Shiga, Japan) for technical support in the estrogenic activity measurements.

References

Alexander, B., Browse, D.J., Reading, S.J., Benjamin, I.S., 1999. A simple and accurate mathematical method for calculation of the EC_{50}. J. Pharmacol. Toxicol. Methods 41, 55–58.

Brandenberger, A.W., Tee, M.K., Jaffe, R.B., 1998. Estrogen receptor alpha (ER-alpha) and beta (ER-beta) mRNAs in normal ovary, ovarian serous cystadenocarcinoma and ovarian cancer cell lines: down-regulation of ER-beta in neoplastic tissues. J. Clin. Endocrinol. Metab. 83, 1025–1028.

Buteau-Lozano, H., Velasco, G., Cristofari, M., Balaguer, P., Perrot-Applanat, M., 2008. Xenoestrogens modulate vascular endothelial growth factor secretion in breast cancer cells through an estrogen receptor-dependent mechanism. J. Endocrinol. 196, 399–412.

Dougherty, E.J., Pollenz, R.S., 2008. Analysis of Ah receptor–ARNT and Ah receptor–ARNT2 complexes in vitro and in cell culture. Toxicol. Sci. 103, 191–206.

Ghisari, M., Bonefeld-Jorgensen, E.C., 2009. Effects of plasticizers and their mixtures on estrogen receptor and thyroid hormone functions. Toxicol. Lett. 189, 67–77.

Ghosh, M.G., Thompson, D.A., Weigel, R.J., 2000. PDZK1 and GREB1 are estrogen-regulated genes expressed in hormone-responsive breast cancer. Cancer Res. 60, 6367–6375.

Hankinson, O., 2008. Why does ARNT2 behave differently from ARNT? Toxicol. Sci. 103, 1–3.

Harrington, W.R., Sheng, S., Barnett, D.H., Petz, L.N., Katzenellenbogen, J.A., Katzenellenbogen, B.S., 2003. Activities of estrogen receptor alpha- and beta-selective ligands at diverse estrogen responsive gene sites mediating transactivation or transrepression. Mol. Cell. Endocrinol. 206, 13–22.

Hatch, E.E., Troisi, R., Wise, L.A., Titus-Ernstoff, L., Hyer, M., Palmer, J.R., Strohsnitter, W.C., Robboy, S.J., Anderson, D., Kaufman, R., Adam, E., Hoover, R.N., 2010. Preterm birth, fetal growth, and age at menarche among women exposed prenatally to diethylstilbestrol (DES). Reprod. Toxicol..

Heldring, N., Pike, A., Andersson, S., Matthews, J., Cheng, G., Hartman, J., Tujague, M., Strom, A., Treuter, E., Warner, M., Gustafsson, J.A., 2007. Estrogen receptors: how do they signal and what are their targets. Physiol. Rev. 87, 905–931.

Hevir, N., Trost, N., Debeljak, N., Rizner, T.L., 2011. Expression of estrogen and progesterone receptors and estrogen metabolizing enzymes in different breast cancer cell lines. Chem. Biol. Interact. 191, 206–216.

Hill, A.J., Heiden, T.C., Heideman, W., Peterson, R.E., 2009. Potential roles of Arnt2 in zebrafish larval development. Zebrafish 6, 79–91.

Hirose, K., Morita, M., Ema, M., Mimura, J., Hamada, H., Fujii, H., Saijo, Y., Gotoh, O., Sogawa, K., Fujii-Kuriyama, Y., 1996. cDNA cloning and tissue-specific expression of a novel basic helix-loop-helix/PAS factor (Arnt2) with close sequence similarity to the aryl hydrocarbon receptor nuclear translocator (Arnt). Mol. Cell. Biol. 16, 1706–1713.

Hosoya, T., Oda, Y., Takahashi, S., Morita, M., Kawauchi, S., Ema, M., Yamamoto, M., Fujii-Kuriyama, Y., 2001. Defective development of secretory neurones in the hypothalamus of Arnt2-knockout mice. Genes Cells 6, 361–374.

Hsu, H.J., Wang, W.D., Hu, C.H., 2001. Ectopic expression of negative ARNT2 factor disrupts fish development. Biochem. Biophys. Res. Commun. 282, 487–492.

Kretzschmar, G., Papke, A., Zierau, O., Moller, F.J., Medjakovic, S., Jungbauer, A., et al., 2010. Estradiol regulates aryl hydrocarbon receptor expression in the rat uterus. Mol. Cell. Endocrinol. 321 (2), 253–257.

Kuiper, G.G., Carlsson, B., Grandien, K., Enmark, E., Haggblad, J., Nilsson, S., Gustafsson, J.A., 1997. Comparison of the ligand binding specificity and transcript tissue distribution of estrogen receptors alpha and beta. Endocrinology 138, 863–870.

Ma, L., 2009. Endocrine disruptors in female reproductive tract development and carcinogenesis. Trends Endocrinol. Metab. 20, 357–363.

Maltepe, E., Keith, B., Arsham, A.M., Brorson, J.R., Simon, M.C., 2000. The role of ARNT2 in tumor angiogenesis and the neural response to hypoxia. Biochem. Biophys. Res. Commun. 273, 231–238.

Martinez, V., Kennedy, S., Doolan, P., Gammell, P., Joyce, H., Kenny, E., Prakash Mehta, J., Ryan, E., O'Connor, R., Crown, J., Clynes, M., O'Driscoll, L., 2008. Drug metabolism-related genes as potential biomarkers: analysis of expression in normal and tumour breast tissue. Breast Cancer Res. Treat. 110, 521–530.

Mitsushima, D., Funabashi, T., Kimura, F., 2003. Estrogen increases messenger RNA and immunoreactivity of aryl-hydrocarbon receptor nuclear translocator 2 in the rat mediobasal hypothalamus. Biochem. Biophys. Res. Commun. 307, 248–253.

Rogers, J.M., Denison, M.S., 2000. Recombinant cell bioassays for endocrine disruptors: development of a stably transfected human ovarian cell line for the detection of estrogenic and anti-estrogenic chemicals. In Vitro Mol. Toxicol. 13, 67–82.

Rogers, J.M., Denison, M.S., 2002. Analysis of the antiestrogenic activity of 2,3,7,8-tetrachlorodibenzo-p-dioxin in human ovarian carcinoma BG-1 cells. Mol. Pharmacol. 61, 1393–1403.

Safe, S., 2004. Endocrine disruptors and human health: is there a problem. Toxicology 205, 3–10.

Scherbakov, A.M., Lobanova, Y.S., Shatskaya, V.A., Krasil'nikov, M.A., 2009. The breast cancer cells response to chronic hypoxia involves the opposite regulation of NF-kB and estrogen receptor signaling. Steroids 74, 535–542.

Schlezinger, J.J., Liu, D., Farago, M., Seldin, D.C., Belguise, K., Sonenshein, G.E., Sherr, D.H., 2006. A role for the aryl hydrocarbon receptor in mammary gland tumorigenesis. Biol. Chem. 387, 1175–1187.

Sekine, H., Mimura, J., Yamamoto, M., Fujii-Kuriyama, Y., 2006. Unique and overlapping transcriptional roles of arylhydrocarbon receptor nuclear translocator (Arnt) and Arnt2 in xenobiotic and hypoxic responses. J. Biol. Chem. 281, 37507–37516.

Sharpe, R.M., Irvine, D.S., 2004. How strong is the evidence of a link between environmental chemicals and adverse effects on human reproductive health? BMJ 328, 447–451.

Sikka, S.C., Wang, R., 2008. Endocrine disruptors and estrogenic effects on male reproductive axis. Asian J. Androl. 10, 134–145.

Swedenborg, E., Pongratz, I., 2010. AhR and ARNT modulate ER signaling. Toxicology 268, 132–138.

Watanabe, M., Yoshida, R., Ueoka, K., Aoki, K., Sasagawa, I., Hasegawa, T., Sueoka, K., Kamatani, N., Yoshimura, Y., Ogata, T., 2007. Haplotype analysis of the estrogen receptor 1 gene in male genital and reproductive abnormalities. Hum. Reprod. 22, 1279–1284.

Welshons, W.V., Thayer, K.A., Judy, B.M., Taylor, J.A., Curran, E.M., vom Saal, F.S., 2003. Large effects from small exposures. I. Mechanisms for endocrine-disrupting chemicals with estrogenic activity. Environ. Health Perspect. 111, 994–1006.

Ziello, J.E., Jovin, I.S., Huang, Y., 2007. Hypoxia-inducible factor (HIF)-1 regulatory pathway and its potential for therapeutic intervention in malignancy and ischemia. Yale J. Biol. Med. 80, 51–60.

In utero exposure to dioxin causes neocortical dysgenesis through the actions of $p27^{Kip1}$

Takayuki Mitsuhashi[a], Junzo Yonemoto[b], Hideko Sone[b], Yasuhiro Kosuge[a,1], Kenjiro Kosaki[a], and Takao Takahashi[a,2]

[a]Department of Pediatrics, School of Medicine, Keio University, Shinjuku-ku, Tokyo 160-8582, Japan; and [b]Research Center for Environmental Risk, National Institute for Environmental Studies, Tsukuba-City, Ibaraki 305-8506, Japan

Edited by Pasko Rakic, Yale University, New Haven, CT, and approved July 13, 2010 (received for review March 8, 2010)

Dioxins have been reported to exert various adverse effects, including cell-cycle dysregulation in vitro and impairment of spatial learning and memory after in utero exposure in rodents. Furthermore, children born to mothers who are exposed to dioxin analogs polychlorinated dibenzofurans or polychlorinated biphenyls have developmental impairments in cognitive functions. Here, we show that in utero exposure to dioxins in mice alters differentiation patterns of neural progenitors and leads to decreased numbers of non-GABAergic neurons and thinner deep neocortical layers. This reduction in number of non-GABAergic neurons is assumed to be caused by accumulation of cyclin-dependent kinase inhibitor $p27^{Kip1}$ in nuclei of neural progenitors. Lending support to this presumption, mice lacking $p27^{Kip1}$ are not susceptible to in utero dioxin exposure. These results show that environmental pollutants may affect neocortical histogenesis through alterations of functions of specific gene(s)/protein(s) (in our case, dioxins), exerting adverse effects by altering functions of $p27^{Kip1}$.

environmental pollutants | cerebral cortex | development | neuronal progenitor cells | cell cycle

Dioxins are ubiquitous environmental pollutants that have been known to disturb hormonal homeostasis in mammals (1–3). In utero exposure to 2,3,7,8-tetrachlorodibenzo-*p*-dioxin (TCDD), one of the most potent dioxins, has been shown to cause impaired spatial learning and memory in rats (4). Furthermore, in humans, it is reported that children born to mothers who are exposed to dioxin analogs polychlorinated dibenzofurans (PCDFs) or polychlorinated biphenyls (PCBs) have developmental impairments in higher cognitive functions (2, 5). Additionally, a recent report describes the relationship between prenatal exposure level of polycyclic aromatic hydrocarbons and child intelligence at 5 y of age (6). However, the mechanisms by which dioxin exposure in utero affects the higher cortical functions after birth remain undetermined.

Non-GABAergic projection neurons, accounting for 80% of the neocortical neurons, are produced by proliferation/differentiation of neuronal progenitor cells (NPCs) constituting the pseudostratified ventricular epithelium [PVE; roughly coexistent with the ventricular zone (VZ)] along the lateral ventricular surface of the embryonic forebrain. The term PVE has been adopted, because it excludes postmitotic, premigratory neuroblasts of the subventricular zone (7, 8). In mice, the NPCs undergo 11 cell divisions during the period of neocortical histogenesis, with the length of the cell cycle (T_C) increasing by 2-fold from 8 to 18 h, mainly because of prolongation of the G1 phase of the cell cycle (T_{G1}) (8). During the same period, the proportion of daughter cells that become postmitotic during each cell cycle [quiescent (Q) fraction] increases (9). It is of critical importance that the layer position of the non-GABAergic projection neurons is strongly correlated with the cell cycle of origin (that is, the cell cycle at which a given non-GABAergic neuron becomes mitotically quiescent and starts radial migration to the neocortex) (10). Taken together, the regulated patterns of increase of the T_{G1} and Q fractions and strict correlation between the layer position and the cell cycle of origin both strongly suggest a link between cell-cycle regulation of the G1 phase and neuronal cell-class determination (layer destination of projection neurons) (10).

Progression of the cell cycle is precisely controlled by a set of proteins including cyclins, cyclin dependent kinases (CDKs), and CDK inhibitors (11). $p27^{Kip1}$, one of the CDK inhibitors, specifically inhibits the activity of cyclin E/CDK2 kinase and inhibits entry of the cells into the S phase (12, 13). Indeed, some of the critical events during the G1 phase of the cell cycle in NPCs are regulated by $p27^{Kip1}$: alterations in $p27^{Kip1}$ expression in the NPCs result in changes in the Q fraction, thereby altering the number of neurons to be produced and hence, the thickness of the neocortex. Specifically, overexpression of $p27^{Kip1}$ in NPCs in vivo increases the Q fraction (that is, promotes differentiation of the NPCs), with a resultant thinner neocortex (14, 15), whereas the lack of $p27^{Kip1}$ decreases the Q fraction, resulting in a thicker neocortex (16). It is worthy of note in this context that TCDD has been reported to induce $p27^{Kip1}$ and delay the G1 phase of the cell cycle in a hepatoma cell line, fetal thymocytes, and human neuronal cell line (17). Taken together, these observations suggest that in utero exposure to TCDD is likely to alter the proliferative behaviors of the NPCs by inducing $p27^{Kip1}$ protein expression, resulting in abnormalities of neocortical histogenesis.

Here, we report that in utero exposure to TCDD indeed modified the $p27^{Kip1}$ activities in NPCs to cause neocortical dysgenesis. These observations can be explained by a hypothetical mathematical model where both the increase in Q fraction and the neuronal class switch occur prematurely compared with that under physiological conditions.

Results

TCDD Exposure in Utero Reduced the Size of the Telencephalon and Thickness of the Neocortex as Assessed on Postnatal Day 21. The telencephalon, olfactory bulb, and cerebellum of TCDD-treated mice showed a normal appearance on postnatal day (P) 21 (Fig. 1*A*). However, the forebrains in these TCDD-treated animals were smaller, with the width and length being reduced by 4.78% (9.48 ± 0.063 mm vs. 9.93 ± 0.030 mm in the controls; $P < 0.001$, $n = 10$) and 2.29% (8.37 ± 0.048 vs. 8.57 ± 0.035 mm; $P = 0.004$, $n = 10$), respectively, compared with the values in the controls. The reductions in the width and length of the telencephalon indicate that TCDD exposure in utero caused roughly 7% reduction of the neocortical surface area. The thickness of the primary somatosensory cortex was reduced by 14.9% (750 ± 29.2 vs. 881.3 ± 13.2 μm; $P < 0.001$, $n = 6$) (Fig. 1*B*); the thickness of the deeper

Author contributions: T.M., J.Y., H.S., K.K., and T.T. designed research; T.M. and Y.K. performed research; T.M. and T.T. analyzed data; and T.M. and T.T. wrote the paper.

The authors declare no conflict of interest.

This article is a PNAS Direct Submission.

Freely available online through the PNAS open access option.

[1]Present address: Research Unit of Pharmacology, School of Pharmacy, Nihon University, Chiba 274-8555, Japan.

[2]To whom correspondence should be addressed. E-mail: ttakahashi@z3.keio.jp.

This article contains supporting information online at www.pnas.org/lookup/suppl/doi:10.1073/pnas.1002960107/-/DCSupplemental.

NEUROSCIENCE

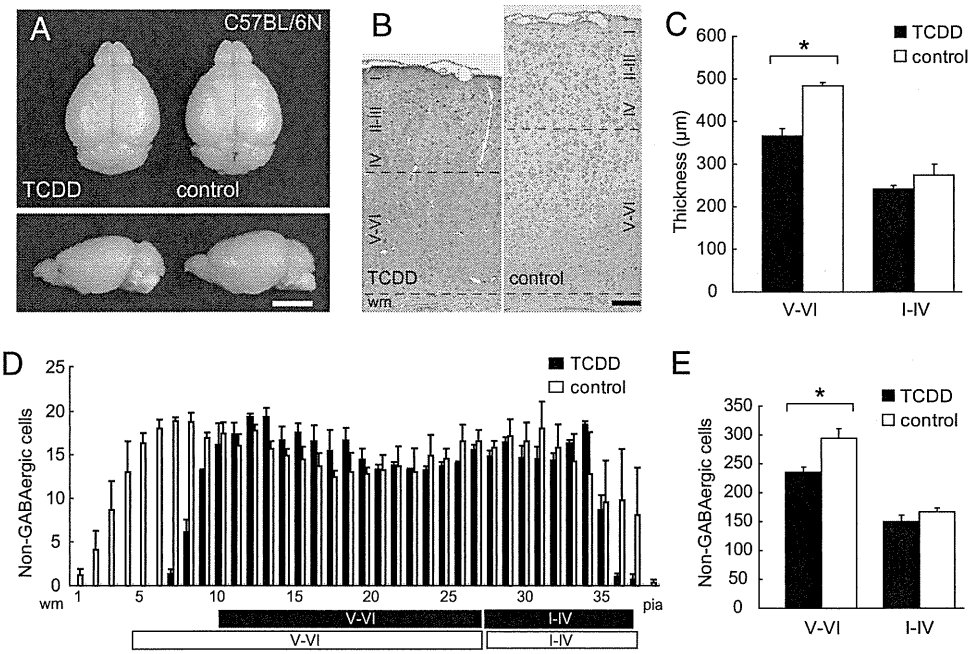

Fig. 1. Effects of in utero TCDD exposure observed on postnatal day 21. (*A*) Macroscopic dorsal and lateral overview of the whole brain from TCDD-treated and control C57BL/6N mice. (Scale bar, 5 mm.) (*B*) High-power view of the primary somatosensory neocortex of the TCDD-treated and control mice. Brown cells, GABA-positive interneurons; purple nuclei, either non-GABAergic projection neurons or glial cells; black dotted lines, boundaries between layers I-IV/V-VI and gray matter/white matter (wm). (Scale bar, 100 μm.) (*C*) Thickness of layers V-VI and I-IV in the TCDD-treated and control mice shown in *B*. (*D*) Numbers of non-GABAergic neurons counted in each bin (250 μm in width and 25 μm in height) lined serially from wm to the pial surface (pia) in the primary somatosensory neocortex shown in *B*. Black and white boxes under the abscissa indicate layers I-IV/V-VI in the neocortex of the TCDD-treated and control mice, respectively. (*E*) Total number of non-GABAergic neurons in layers V-VI and I-IV. $*P < 0.05$. Error bars in *C–E*, SEM.

cortical layers (layers V-VI) was reduced by 24.1% (366.7 ± 16.67 vs. 483.3 ± 8.33 μm; $P = 0.005$, $n = 6$), whereas no significant change in the thickness of the superficial layers (layers I-IV) was noted (241.7 ± 8.33 vs. 275.0 ± 25.0 μm; $P = 0.38$, $n = 6$) (Fig. 1*C*).

TCDD Exposure in Utero Reduced the Number of Non-GABAergic Neurons in the Deeper Cortical Layers as Assessed on Postnatal Day 21. We identified non-GABAergic projection neurons by the lack of positive immunohistochemical staining of the cells with anti-GABA antibody (Fig. 1 *B* and *D*). The number of non-GABAergic projection neurons in the primary somatosensory neocortex on P21 was significantly reduced in the deeper layers of the TCDD-treated animals by 20.0% compared with that in normal controls (Fig. 1*E*) (235.6 ± 9.24 vs. 294.3 ± 16.9 per 1,000 μm^2; $P = 0.037$, $n = 3$). However, there was no significant difference in the number of non-GABAergic neurons in the superficial layers of the cortex in the TCDD-treated animals compared with that in the controls (Fig. 1*E*) (149.8 ± 10.9 vs. 166.8 ± 6.14 per 1,000 μm^2; $P = 0.246$, $n = 3$). No alteration in the cell-packing density of the non-GABAergic projection neurons was observed in either the deeper or superficial layers in the TCDD-treated animals. Taken together, we concluded that the reduction in neocortical thickness of the TCDD-treated mice was caused by the reduction in the number of non-GABAergic projection neurons in the deeper cortical layers.

Total Cell Cycle Length of the NPCs Was Not Altered by TCDD Exposure in Utero. Next, we examined the TCDD-treated embryonic forebrains on E12, the time point at which the non-GABAergic neurons of the deeper layers (layers V–VI) are to be produced (10). Histologically, the dorsomedial cerebral wall, the future primary somatosensory neocortex, was normal in the TCDD-treated embryos (Fig. 2*A*). The S phase zone, where accumulation of the nuclei of the NPCs is observed during the S phase of the cell cycle, in the dorsomedial cerebral wall was located between 60 and 70 μm from the lateral ventricular border on E12 in the TCDD-treated mice, similar to the finding in the normal control mice (Fig. 2 *A* and *B*) ($n = 4$). At 4 h after exposure to bromodeoxyuridine (BrdU), BrdU-positive nuclei moved to the ventricular surface in both the TCDD-treated and control animals, indicating that the interkinetic nuclear migration in the embryonic forebrain operated normally in the TCDD-treated mice (Fig. 2*C*) ($n = 3$). After 6.5 h exposure to BrdU, virtually all of the nuclei in the VZ were BrdU-positive in both the TCDD-treated and control mice, indicating that the growth fractions in the VZ were nearly equal to 1.0 in both the TCDD-treated and control mice (Fig. 2*D*) ($n = 3$). The results of cumulative BrdU labeling (Fig. 2*E*) (18) revealed that the total cell-cycle length of the NPCs in the forebrain of the TCDD-treated animals was 10.7 h, not significantly different from that in the controls (Table 1).

TCDD Exposure in Utero Promoted Early Cell Cycle Exit of NPCs. We then identified the NPCs in the Q fraction and P fraction (the fraction of daughter cells that remain proliferative; $P = 1.0 - Q$) on E12 by using two S-phase tracers, iododeoxyuridine (IdU) and BrdU (Fig. 2*F*) (15, 19). In the dorsomedial cerebral wall of the TCDD-treated mice, the IdU-positive nuclei (blue nuclei) were located in the outer margin of the S-phase zone in both the P + Q and Q experiments (Fig. 2*F*). The distribution patterns of the P + Q and Q cells were not different between the TCDD-treated and control animals (Fig. 2*G*). An increase in the number of Q cells was observed in the TCDD-treated animals, with an estimated Q fraction of 0.17, which represented a 21.4% increase compared with the value in the controls (Table 2) ($n = 3$).

TCDD Exposure in Utero Increased the Nuclear Fraction of the $p27^{Kip1}$ Protein in the NPCs. To elucidate the molecular mechanisms underlying the aforementioned changes, we first investigated the TCDD-induced changes in the mRNA expression levels of cell-cycle regulatory genes in the dorsomedial cerebral wall by dot blot hybridization (Fig. 3 *A* and *B*) ($n = 5$). We observed up-regulation

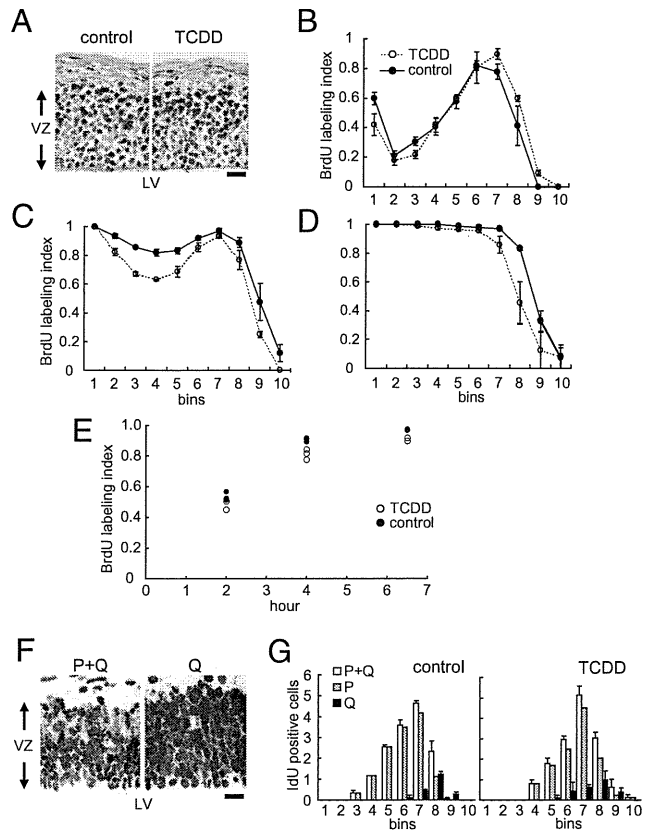

Fig. 2. Effects of in utero TCDD exposure on the cell-cycle kinetics of the NPCs. (*A*) High-power views of the dorsomedial cerebral wall of the E12 forebrains of the control and TCDD-treated mice. Black, BrdU-labeled nuclei; red, non–BrdU-labeled nuclei; VZ, ventricular zone; LV, lateral ventricle. (Scale bar, 10 μm.) (*B*) The 2-h BrdU-labeling index was evaluated in each bin (100 μm in width and 10 μm in height) lined serially from the lateral ventricle to the pial surface in the ventricular zone. The 4-h (*C*) and 6.5-h (*D*) BrdU-labeling indices are also shown. (*E*) Total labeling indices after cumulative BrdU exposure. (*F*) High-power views of the dorsomedial area of the E12 forebrains of mice exposed to TCDD. Blue nuclei, IdU-only positive; brown nuclei, double positive for IdU and BrdU. In the P + Q experiment (*Left*), blue nuclei correspond to the P + Q fraction cells. In the Q experiment (*Right*), blue cells correspond to only the Q fraction cells. (Scale bar, 10 μm.) (*G*) The number of Q fraction cells and P + Q fraction cells that were counted in each bin in control (*Left*) and TCDD-treated embryos (*Right*).

of the *p27*^{Kip1} and *p15*^{INK4b} mRNAs in the E12 forebrain in the TCDD-treated animals compared with the expressions in the controls (Fig. 3*B*): both *p27*^{Kip1} and *p15*^{INK4b} are CDK inhibitors that are known to promote exit from the cell cycle (11). We then analyzed the p27^{Kip1} and p15^{INK4b} protein levels by immunoblot analysis of lysates of the E12 dorsomedial cerebral walls. The p27^{Kip1} and p15^{INK4b} protein levels in the total tissue lysate were not significantly different between the TCDD-treated and control animals. However, when only the nuclear fractions from the dorsomedial cerebral wall were analyzed, the p27^{Kip1} protein level was

Table 1. Lengths of each phase of the cell cycle estimated by cumulative BrdU labeling index

	$T_C - T_S$	T_C	T_S	T_{G1}	T_{G2+M}
TCDD	7.0	10.7	3.7	5.0	2.0
Control	6.3	10.5	4.3	4.3	2.0

T_C, length of the total cell cycle; T_S, length of S phase, T_{G1}, length of G1 phase; T_{G2+M}, length of G2 + M phase.

Table 2. Q fraction analysis

	N_{P+Q}	N_Q	P fraction	Q fraction
TCDD	14.5	2.6	0.82	0.17
Control	14.7	2.1	0.86	0.14

N_{P+Q}, number of blue nuclei in the P + Q experiment; N_Q, number of blue nuclei in the Q experiment; Q fraction, N_Q/N_{P+Q}; P fraction, 1 − Q.

about 2.5-fold higher in the TCDD-treated mice compared with the levels in the controls, the difference being significant (Fig. 3 *C* and *D*) ($n = 4$).

TCDD Exposure in Utero Did Not Reduce the Number of Non-GABAergic Neurons in the Deeper Cortical Layers of the p27^{Kip1} Knockout Mice. To further confirm the role of p27^{Kip1} in the events associated with TCDD exposure in utero, we repeated the in utero TCDD exposure experiments using p27^{Kip1} knockout mice (p27$^{-/-}$) (Fig. 4*A*) (20–22). We have previously reported that an increased thickness of the somatosensory neocortex on P21 in p27$^{-/-}$ mice compared with that in the wild-type animals is caused by the overproduction of non-GABAergic projection neurons destined for the superficial neocortical layers (16). Here, neither the layer thickness nor the number in non-GABAergic neurons of the primary somatosensory neocortex on P21 was significantly reduced in the TCDD-treated p27$^{-/-}$ compared with the findings in the controls (i.e., p27$^{-/-}$ mice exposed to corn oil; $n = 5$) (Fig. 4 *B–D*).

Discussion

Reduction in the Peak Population Size of NPCs by TCDD Exposure. The neocortical surface area, although influenced by multiple factors such as neuropil expansion and other growth-related parameters, is mostly determined during its ontogeny by the degree of tangential expansion of PVE (9). The size of the PVE, in turn, is virtually exclusively determined by the maximum population size of the NPCs, because dominant constituents of the PVE are the NPCs (9). Thus, the reduction of the neocortical surface area in the TCDD-treated mice (Fig. 1) strongly indicates a decrease in the maximum number of NPCs during neocortical histogenesis. The population size of the NPCs is governed solely by the pattern of ascent of the Q fraction during the early phase of neocortical histogenesis, and the maximum size is reached at the

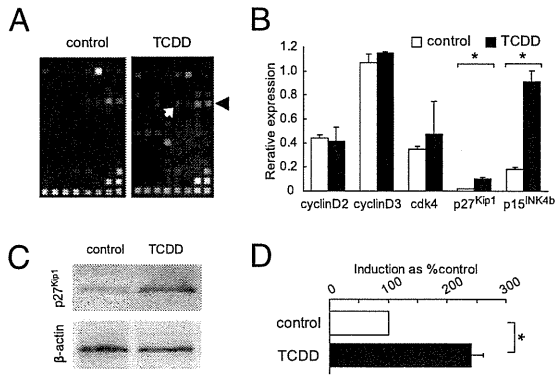

Fig. 3. Effects of in utero TCDD exposure on the expression profile of cell-cycle regulatory genes in the NPCs. (*A*) cDNA expression arrays hybridized with biotinylated probes generated from the embryonic forebrain of control and TCDD-treated mice. Black arrowhead and white arrow indicate signals from *p15*^{INK4b} and *p27*^{Kip1}, respectively. (*B*) mRNA expression after TCDD exposure. The β-actin signal equals 1.0. (*C*) Immunoblot analysis of nuclear p27^{Kip1} protein in the forebrains of the embryos of the control and TCDD-treated mice. β-actin levels were used to verify equal loading of the samples. (*D*) TCDD-induced increase of nuclear p27^{Kip1} protein. Bars, percentage signal intensity relative to the levels in the control embryos set at 100%. *$P < 0.05$. Error bars in *B* and *D*, SEM.

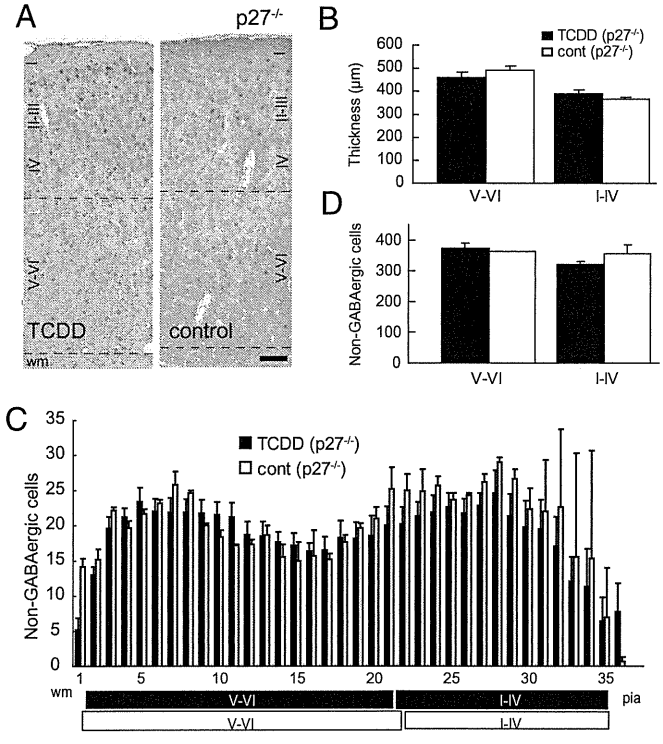

Fig. 4. Effects of in utero TCDD exposure in $p27^{Kip1}$ knockout mice as assessed on P21. (*A*) High-power view of the primary somatosensory neocortex of $p27^{Kip1}$ knockout mice ($p27^{-/-}$) exposed to TCDD and control mice. Brown cells, GABA-positive interneurons; purple nuclei, either non-GABAergic projection neurons or glial cells; black dotted lines, boundaries between layers I-IV/V-VI and gray matter/wm. (Scale bar, 100 μm.) (*B*) Thickness of layers V-VI and I-IV in the TCDD-treated and control mice shown in *A*. (*C*) Numbers of non-GABAergic neurons counted in each bin (250 μm in width and 25 μm in height) lined serially from the wm to the pia in the primary somatosensory neocortex shown in *A*. Black and white boxes under the abscissa indicate layers I-IV/V-VI in the neocortex of the TCDD-treated and control mice, respectively. (*D*) Total number of non-GABAergic neurons in layers V-VI and I-IV. Error bars in *B–D*, SEM.

point where the Q fraction reaches 0.5: the earlier the Q fraction reaches 0.5, the smaller the peak NPC population size (9, 23). Because no increase in apoptosis was noted in the PVE of the TCDD-treated mice, we conclude that TCDD exposure in utero reduced the peak population size of the NPCs by inducing a premature increase of the Q fraction. Because the degree of surface-area reduction is relatively small (7%), the premature increase in the Q fraction to 0.5 was likely to have occurred relatively late during the period, when the Q fraction was between 0 and 0.5. This assumption agrees with the previously reported $p27^{Kip1}$ expression pattern among NPCs (that is, extremely low at the outset with the peak expression in the middle of neuronogenesis) (24).

Possible Mechanisms of Underproduction of Non-GABAergic Neurons in the Deeper Cortical Layers. It is of critical importance to note that only those projection neurons that are produced during the early phase of neuronogenesis when the Q fraction is less than 0.5 become destined for the deeper cortical layers (9, 10). It follows that the time point at which the Q fraction reaches 0.5 during neuronogenesis is the critical time window for the phenotypic switch from the deep- to superficial-layer neurons (25). Taken together, we conclude that the abnormal increase of the Q fraction during the early phase of neuronogenesis induced by TCDD exposure leads not only to a decrease of the peak population size of the NPCs but also to premature-cell phenotype switch and consequently, a decrease in the number of non-GABAergic projection neurons in the deeper cortical layers.

Of note, the progenitor population of the PVE is already committed to their lineage without pluripotency. In fact, our preliminary results indicated that GABAergic neurons and glial cells were also reduced in number, and such reduction was not observed in $p27^{-/-}$. It follows that $p27^{Kip1}$ is likely to be responsible for determining the size of those neural populations as well. The proliferation/differentiation characteristics of progenitor populations of GABAergic neurons (NPCs of the ganglionic eminence) and glial cells surely deserve further investigation (26).

Mechanism of Nuclear Accumulation of $p27^{Kip1}$ After TCDD Exposure. The premature increase of the Q fraction, as described in the foregoing paragraphs, is the underlying biological mechanism for the TCDD-induced abnormality of neocortical histogenesis. The increase of the Q fraction seems to be attributable to the nuclear accumulation of $p27^{Kip1}$: this hypothesis is lent strong support by the finding that mice lacking the $p27^{Kip1}$ protein showed almost no alteration of the neocortical thickness after TCDD exposure (Fig. 4). Thus, $p27^{Kip1}$ may be involved in the cascade of critical events anywhere downstream of the direct effect of TCDD. There has been no report to this date, to the best of our knowledge, on the effect of TCDD on the subcellular localization of the $p27^{Kip1}$. The nuclear fraction of $p27^{Kip1}$ protein is determined by the balance of the protein transportation into and out of the nuclei. However, the expression levels of Jab-1, Akt, and Skp2 proteins, known to be involved in the nuclear transportation and degradation of the $p27^{Kip1}$ protein, were not found to be altered in the NPCs of the TCDD-treated mice (27–31). Another intriguing observation is the stability of the total cell-cycle length observed, despite TCDD exposure (Table 1). The stabilizing mechanisms of the cell-cycle kinetics shown in *Drosophila melanogaster* (32) may also be involved in the homeostasis of the NPC cell cycle after in utero TCDD exposure.

This report quantitatively evaluates the effects of an environmental pollutant on neocortical histogenesis. In addition, this study is an example of an experimental model where the phenotypic severity of a particular adverse effect of a given environmental substance was found to be dependent on the genotype of the animals, which has profound implications from the viewpoint of toxicogenomics (33). Furthermore, our mathematical model of neocortical histogenesis has been shown to be a powerful tool to examine neocortical dysgenesis after relatively subtle alterations in the decision-making characteristics of the NPCs. We believe that this analytical method would be applicable to various environmental substances that may have adverse effects on human CNS development.

Materials and Methods

TCDD Administration. TCDD (Cambridge Isotope Laboratory) was dissolved in corn oil at a concentration of 2 μg mL^{-1}. A single dose of TCDD solution, or corn oil {0.01 mL [gram body weight (g bw)]$^{-1}$} as control, was administered orally to pregnant C57BL/6N and $p27^{-/-}$ mice on E7 using a disposable feeding needle. The total dose of TCDD administered was 20 μg (kg bw)$^{-1}$. This dose was adopted, because it was expected not to affect the mother in terms of child-rearing behavior. In fact, no adverse effect was observed during pregnancy and the postpartum period.

Measurement of the Dimensions of the Telencephalon. Brains from either TCDD- or corn oil-exposed mice on P21 were fixed in 4% phosphate-buffered formaldehyde containing 0.5% glutaraldehyde by transcardiac perfusion. The length and width of 10 telencephalons obtained from either TCDD- or corn oil-exposed P21 mice embryos were measured with micrometer calipers.

GABA Immunohistochemistry, Cumulative BrdU Labeling Analysis, and Q Fraction Analysis. GABA immunohistochemistry was performed as described previously using anti-GABA antibody (Chemicon International) (16). Cumulative BrdU labeling analysis (18) and Q fraction analysis (9, 15, 34) were performed as previously described. Detailed methods are described in *SI Materials and Methods*.

mRNA Expression Analysis and Immunoblot Analysis. Total RNA was isolated from E12 cerebral walls using the RNeasy Protect kit (Qiagen), and the mRNA was purified using the MicroPolyA Pure kit (Ambion) for generating biotinylated cDNA probes. The biotinylated probes were hybridized to cDNA expression arrays (GE array Q series Mouse Cell Cycle Gene Array; Superarray). Immunoblot analyses were conducted using anti-$p27^{Kip1}$, $p15^{INK4b}$, cyclin E, Skp2, β-actin (Santa Cruz Biotechnology), cyclin D1, CDK2, CDK4 (Sigma), AKT (Cell Signaling Technology), and Jab-1 (GeneTex) antibodies. Detailed methods are described in *SI Materials and Methods*.

ACKNOWLEDGMENTS. $p27^{Kip1}$ knockout mice were provided by Nippon Roche K.K. which were generated by Nakayama K, et al. (20). We acknowledge the assistance of Ms. H. Zaha and the discussions that we held with Drs. C. Tohyama and T. Goto during the preparation of this manuscript. This work was supported by Grant-in-Aid for Young Scientists (B) of the Ministry of Education, Culture, Sports, Science and Technology of Japan (17790723, 20790744, and 22791001 to T.M.) and Grant-in-Aid for Scientific Research (B) of Japan Society for the Promotion of Science (JSPS) (15390327, 18390302, and 20390299 to T.T.) and the 21st century Center of Excellence program of JSPS.

1. Barsotti DA, Abrahamson LJ, Allen JR (1979) Hormonal alterations in female rhesus monkeys fed a diet containing 2,3,7,8-tetrachlorodibenzo-p-dioxin. *Bull Environ Contam Toxicol* 21:463–469.
2. Birnbaum LS (1994) Endocrine effects of prenatal exposure to PCBs, dioxins, and other xenobiotics: Implications for policy and future research. *Environ Health Perspect* 102: 676–679.
3. Poland A, Knutson JC (1982) 2,3,7,8-tetrachlorodibenzo-p-dioxin and related halogenated aromatic hydrocarbons: Examination of the mechanism of toxicity. *Annu Rev Pharmacol Toxicol* 22:517–554.
4. Markowski VP, Cox C, Preston R, Weiss B (2002) Impaired cued delayed alternation behavior in adult rat offspring following exposure to 2,3,7,8-tetrachlorodibenzo-p-dioxin on gestation day 15. *Neurotoxicol Teratol* 24:209–218.
5. Chen YC, Guo YL, Hsu CC, Rogan WJ (1992) Cognitive development of Yu-Cheng ("oil disease") children prenatally exposed to heat-degraded PCBs. *JAMA* 268:3213–3218.
6. Perera FP, et al. (2009) Prenatal airborne polycyclic aromatic hydrocarbon exposure and child IQ at age 5 years. *Pediatrics* 124:e195–e202.
7. Sauer FC (1935) Mitosis in the neural tube. *J Comp Neurol* 62:377–405.
8. Takahashi T, Nowakowski RS, Caviness VS, Jr (1995) The cell cycle of the pseudostratified ventricular epithelium of the embryonic murine cerebral wall. *J Neurosci* 15:6046–6057.
9. Takahashi T, Nowakowski RS, Caviness VS, Jr (1996) The leaving or Q fraction of the murine cerebral proliferative epithelium: a general model of neocortical neuronogenesis. *J Neurosci* 16:6183–6196.
10. Takahashi T, Goto T, Miyama S, Nowakowski RS, Caviness VS, Jr (1999) Sequence of neuron origin and neocortical laminar fate: Relation to cell cycle of origin in the developing murine cerebral wall. *J Neurosci* 19:10357–10371.
11. Sherr CJ, Roberts JM (1999) CDK inhibitors: Positive and negative regulators of G1-phase progression. *Genes Dev* 13:1501–1512.
12. Toyoshima H, Hunter T (1994) p27, a novel inhibitor of G1 cyclin-Cdk protein kinase activity, is related to p21. *Cell* 78:67–74.
13. Polyak K, et al. (1994) Cloning of p27Kip1, a cyclin-dependent kinase inhibitor and a potential mediator of extracellular antimitogenic signals. *Cell* 78:59–66.
14. Mitsuhashi T, et al. (2001) Overexpression of p27Kip1 lengthens the G1 phase in a mouse model that targets inducible gene expression to central nervous system progenitor cells. *Proc Natl Acad Sci USA* 98:6435–6440.
15. Tarui T, et al. (2005) Overexpression of p27 Kip 1, probability of cell cycle exit, and laminar destination of neocortical neurons. *Cereb Cortex* 15:1343–1355.
16. Goto T, Mitsuhashi T, Takahashi T (2004) Altered patterns of neuron production in the p27 knockout mouse. *Dev Neurosci* 26:208–217.
17. Kolluri SK, Weiss C, Koff A, Göttlicher M (1999) p27(Kip1) induction and inhibition of proliferation by the intracellular Ah receptor in developing thymus and hepatoma cells. *Genes Dev* 13:1742–1753.
18. Takahashi T, Nowakowski RS, Caviness VS, Jr (1992) BUdR as an S-phase marker for quantitative studies of cytokinetic behaviour in the murine cerebral ventricular zone. *J Neurocytol* 21:185–197.
19. Nowakowski RS, Lewin SB, Miller MW (1989) Bromodeoxyuridine immunohistochemical determination of the lengths of the cell cycle and the DNA-synthetic phase for an anatomically defined population. *J Neurocytol* 18:311–318.
20. Nakayama K, et al. (1996) Mice lacking p27(Kip1) display increased body size, multiple organ hyperplasia, retinal dysplasia, and pituitary tumors. *Cell* 85:707–720.
21. Kiyokawa H, et al. (1996) Enhanced growth of mice lacking the cyclin-dependent kinase inhibitor function of p27(Kip1). *Cell* 85:721–732.
22. Fero ML, et al. (1996) A syndrome of multiorgan hyperplasia with features of gigantism, tumorigenesis, and female sterility in p27(Kip1)-deficient mice. *Cell* 85: 733–744.
23. Takahashi T, Nowakowski RS, Caviness VS, Jr (1997) The mathematics of neocortical neuronogenesis. *Dev Neurosci* 19:17–22.
24. Delalle I, Takahashi T, Nowakowski RS, Tsai LH, Caviness VS, Jr (1999) Cyclin E-p27 opposition and regulation of the G1 phase of the cell cycle in the murine neocortical PVE: A quantitative analysis of mRNA in situ hybridization. *Cereb Cortex* 9:824–832.
25. Caviness VS, Jr, et al. (2003) Cell output, cell cycle duration and neuronal specification: A model of integrated mechanisms of the neocortical proliferative process. *Cereb Cortex* 13:592–598.
26. Bhide PG (1996) Cell cycle kinetics in the embryonic mouse corpus striatum. *J Comp Neurol* 374:506–522.
27. Tomoda K, et al. (2002) The cytoplasmic shuttling and subsequent degradation of p27Kip1 mediated by Jab1/CSN5 and the COP9 signalosome complex. *J Biol Chem* 277: 2302–2310.
28. Kossatz U, et al. (2004) Skp2-dependent degradation of p27kip1 is essential for cell cycle progression. *Genes Dev* 18:2602–2607.
29. Carrano AC, Eytan E, Hershko A, Pagano M (1999) SKP2 is required for ubiquitin-mediated degradation of the CDK inhibitor p27. *Nat Cell Biol* 1:193–199.
30. Nakayama K, et al. (2000) Targeted disruption of Skp2 results in accumulation of cyclin E and p27(Kip1), polyploidy and centrosome overduplication. *EMBO J* 19:2069–2081.
31. Liang J, et al. (2002) PKB/Akt phosphorylates p27, impairs nuclear import of p27 and opposes p27-mediated G1 arrest. *Nat Med* 8:1153–1160.
32. Reis T, Edgar BA (2004) Negative regulation of dE2F1 by cyclin-dependent kinases controls cell cycle timing. *Cell* 117:253–264.
33. Shih DM, et al. (1998) Mice lacking serum paraoxonase are susceptible to organophosphate toxicity and atherosclerosis. *Nature* 394:284–287.
34. Hayes NL, Nowakowski RS (2000) Exploiting the dynamics of S-phase tracers in developing brain: Interkinetic nuclear migration for cells entering versus leaving the S-phase. *Dev Neurosci* 22:44–55.

Review

Oxygenomics in environmental stress

H. Sone[1], H. Akanuma[1], T. Fukuda[2]

[1]National Institute for Environmental Studies, Tsukuba, Ibaraki, Japan
[2]Tohoku University, Aoba-ku, Sendai, Japan

Environmental stressors such as chemicals and physical agents induce various oxidative stresses and affect human health. To elucidate their underlying mechanisms, etiology and risk, analyses of gene expression signatures in environmental stress-induced human diseases, including neuronal disorders, cancer and diabetes, are crucially important. Recent studies have clarified oxidative stress-induced signaling pathways in human and experimental animals. These pathways are classifiable into several categories: reactive oxygen species (ROS) metabolism and antioxidant defenses, p53 pathway signaling, nitric oxide (NO) signaling pathway, hypoxia signaling, transforming growth factor (TGF)-β bone morphogenetic protein (BMP) signaling, tumor necrosis factor (TNF) ligand–receptor signaling, and mitochondrial function. This review describes the gene expression signatures through which environmental stressors induce oxidative stress and regulate signal transduction pathways in rodent and human tissues.

Keywords: Oxygenomics, environmental stress, gene expression signatures, signal transduction pathways

Introduction

Oxidative stress in the form of excess reactive oxygen species (ROS) or reactive nitrogen species (RNS) can affect cells deleteriously or beneficially. Such stress might be generated by intracellular or extracellular sources. Furthermore, oxidative stress can cause various human diseases. Environmental stress is a key contributor to human disease. Myriad substances such as metals, particulate materials, smoke, pesticides, and physical agents are environmental stressors (see Table 1) that contribute to many diseases. Concerns related to environmental stressor-related diseases such as cancer, chronic lung disease, diabetes mellitus, neurodegenerative diseases, and reproductive disorders have been raised recently. Research efforts elucidating the modes by which environmental stressors influence the development and progression of diseases or exploring preventive approaches are expected to engender further improvements in our knowledge. Understanding environmental stressor-induced influences at the molecular level will also provide a wealth of information related to the exploration of biomarkers for environmental stressor-related diseases.[1–3]

The mechanisms of redox adaptation in living bodies and cells might involve multiple influences on an active redox-sensitive signaling pathway, such as ROS metabolism and antioxidant defenses, p53 pathway signaling, nitric oxide (NO) signaling pathway, hypoxia signaling, transforming growth factor (TGF)-β-bone morphogenetic protein (BMP) signaling, tumor necrosis factor (TNF) ligand–receptor signaling, and mitochondrial function (Table 2). For example, transcription factors such as nuclear factor-κB (NF-κB), nuclear factor erythroid 2-related factor 2 (Nrf2), c-Jun and hypoxia-inducible factor-1 (HIF-1) engender increased expression of anti-oxidant molecules such as superoxide dismutase (SOD), catalase, thioredoxin, and the GSH antioxidant system. Metal ions such as arsenic(III/V)

Correspondence to: Correspondence to: Dr Hideko Sone, National Institute for Environmental Studies, 16-2 Onogawa, Tsukuba, Ibaraki, Japan
E-mail: hsone@nies.go.jp
Received 12 December 2009, manuscript accepted 9 April 2010

DOI 10.1179/174329210X12650506623843

Table 1 Environmental stressors that induce oxidative stress

Sources	
Metals	Antimony (Sb), arsenic (As), beryllium (Be), cadmium (Cd), chromium (Cr), cobalt (Co), copper (Cu), lead (Pb), mercury (Hg), nickel (Ni), vanadium (V)
Particulate matter and smoke	PM10, PM2.5, carbon monoxide (CO) sulfur dioxide (SO_2), nitrogen oxides (NOx), ozone (O_3), asbestos
Agriculture-related chemicals	Pesticides, fungicides
Persistent organic pollutants	Aldrin, chlordane, DDT, dieldrin, endrin, heptachlor, hexachlorobenzene, mirex, polychlorinated biphenyls, polychlorinated dibenzo-*p*-dioxins, polychlorinated dibenzofurans, toxaphene, carcinogenic polycyclic aromatic hydrocarbons, certain brominated flame-retardants, organometallic compounds such as tributylin TBT
Hormones and environmental hormones (endocrine disrupting chemicals)	Estradiol, dehydrotestosterone, bisphenols, phthalates
Physical agents	Burn Radiation UV radiation

or copper(II) directly influence expression levels of those transcription factors and induce various oxidative stress events including thiol molecule perturbation, generation of oxidative DNA adducts, and induction of oxidative molecular biomarkers.[4–7] Non-metal chemicals such as retinoic acids and 2,3,7,8-tetrachlorodibenzo-*p*-dioxin (TCDD) are also known to influence the expression of oxidative stress-related genes and proteins during carcinogenesis and during embryonic development.[8–11] In relation to cancer, a growing tumor might also produce intracellular and extracellular oxidative stress, which can modify its malignant features. Endogenous sources of tumor ROS or RNS include impaired intracellular genomes or proteomes, metabolism pathways, and xenobiotic metabolism. Consequently, the study of transcriptional regulation of gene expression in the research field of oxidative stress has been useful for identifying new *trans*-regulatory factors or new biomarkers induced by exposure to environmental stressors.

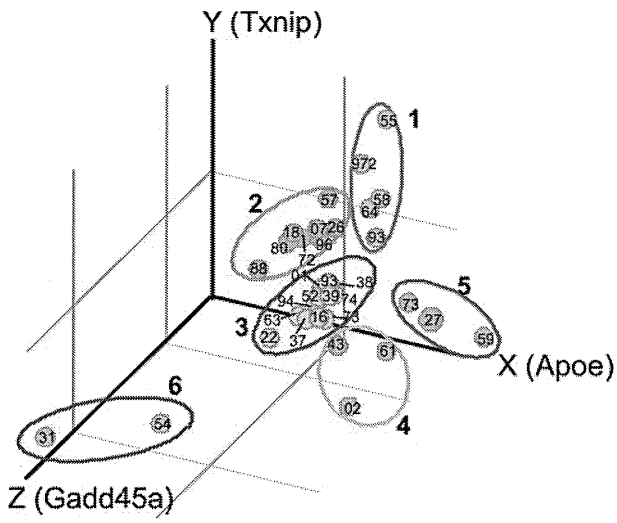

Figure 1 Principal component analysis of oxidative stress-induced genes extracted from 33 independent datasets in GEO. Numbers indicate the last two or three digits of GEOID

Microarray technology has been used in environmental toxicology and biology studies and has led to the establishment of gene expression signatures profiling the toxicity of environmental stressors.[12,13] Statistical methods used for DNA microarray studies are mostly multivariate approaches. Although basic methods treat genes as traits, which are consistent with the rules of experimental design, several approaches have been developed using expression ratio datasets. Such approaches regard the genes as cases and the array plates as variables. Most well-known methods based on singular value decomposition have used principal component analysis (Fig. 1).[14,15] In alternative approaches, our previous reports have described that a Bayesian network technique, which is a probabilistic graphical model that represents a set of variable identities, is applicable to investigation of the gene expression interaction networks and the detection of differences arising in them from exposure to different doses of chemicals.[16,17] Bayesian network techniques can provide predictive information related to the relations between agents and gene expression signatures in life science fields.[18–20]

Toyokuni[21] first proposed a new science field – oxygenomics – which is defined as a research area

Table 2 Core oxidative stress pathways

Categorical pathway Canonical pathway (orthology)
Reactive oxygen species (ROS) metabolism and antioxidant defenses
• Glutathione peroxidases (GPx)
• Peroxiredoxins (TPx)
• Superoxide dismutases (SOD)
• Genes involved in superoxide metabolism
• Genes involved in ROS metabolism
• Other peroxidases and antioxidant-related genes
p53 signaling (including DNA damage)
• Apoptosis-related genes
• Cell cycle arrest and checkpoint
• Regulation of the cell cycle
• Regulation of cell proliferation, cell growth and differentiation
• Damaged DNA binding
• Mismatch, base-excision and double-strand break repair
Nitric oxide (NO) signaling pathway
• Genes with NO synthase and regulators of NO biosynthesis
• Genes regulated by NO and NO signaling pathway
• Genes involved in superoxide release
• Anti-apoptosis genes
• Genes with antioxidant and superoxide dismutase activity
• Genes with glutathione peroxidase, oxidoreductase, peroxidase activity
• Transcription regulators
Hypoxia signaling
• Response to hypoxia and signal transduction, oxidative stress
• Genes related to stress and immune response
• Hemoglobin complex associated Genes
• Peroxidase, oxidoreductase-related genes
• Transcription factors and regulators and protein binding
• Anti-apoptosis
• Induction of apoptosis and caspase activity
• Protein biosynthesis, phosphorylation and metabolism
• Cytoskeleton and other extracellular molecules
• Cell cycle, cell proliferation and growth factors
• Carbohydrate, lipid, one-carbon compound metabolism
• RNA metabolism
• Cardiac excitation–contraction (E–C) coupling
TGF-β-BMP signaling
• TGF-β superfamily, bone morphogenetic protein (BMP) family members, growth differentiation factor (GDF), activin, and activin receptors
• SMAD family members, TGF-β/activin-responsive genes, BMP-responsive genes, molecules regulating signaling of the TGF-β superfamily, adhesion molecules, extracellular matrix structural constituents, other extracellular molecules, transcription factors and regulators
Tumor necrosis factor (TNF) ligand–receptor signaling
• Caspase activation, caspase inhibition, anti-apoptosis genes, induction of apoptosis, other apoptosis-related genes, JNK signaling pathway, NF-κB signaling pathway, TNF superfamily members, TNFr1 and TNFr2 signaling pathway, inflammatory response, transcription regulators
Mitochondria
• Mitochondrial processing, mitochondrial transportation, fatty acid biosynthesis

studying the localization of oxidative DNA damage in the genomes of living cells. Oxygenomics is becoming a significant strategy for discovery of important biomarkers and for evaluation of risks and effects.

This review addresses various environmental stressor-induced toxicities in rats and humans to elucidate the molecular mechanisms underlying toxicity-induced oxidative stress.

Categorical pathways in oxygenomics

Cells respond and adapt to environmental signals, such as stressors,[22–24] through multiple mechanisms that involve communication pathways and signal transduction processes. The impact of oxidative stress on various diseases and aging has been reviewed comprehensively. In particular, free-radical-induced oxidative stress plays an important role in cancer development, aging, and some toxicant-induced apoptosis.[3,25,36] Our survey of microarray databases and many other published references has revealed the categorical pathways induced by oxidative stress, as presented in Table 2.

ROS metabolism and antioxidant defenses center upon ROS, which are necessary for biological functions and which regulate many signal transduction pathways by directly reacting with and modifying the structure of proteins, transcription factors, and genes to modulate their functions. Actually, ROS induce expression levels of genes associated with signaling cell growth and differentiation, regulating the activity of enzymes (such as ribonucleotide reductase and peroxidase). Control of ROS levels is achieved by balancing ROS generation with their elimination through ROS-scavenging systems such as superoxide dismutases (SOD1, SOD2, and SOD3), glutathione peroxidase, peroxiredoxins, glutaredoxin, and thioredoxin catalase. The ROS can modulate the activities and expression of many transcription factors and signaling and signaling proteins that are involved in stress response and cell survival through multiple mechanisms. Therefore, this category includes glutathione peroxidases (GPx), peroxiredoxins (TPx), superoxide dismutases (SOD), genes involved in superoxide metabolism such as arachidonate 12-lipoxygenase (ALOX12), and copper chaperone for superoxide dismutase (CCS). In fact, p53 signaling plays a central role in co-ordinating the cellular responses to a broad range of cellular stress factors: p53 functions as a node for organizing whether the cell